International Journal of Nanomedicine

Dovepress
Taylor & Francis Group

Open Access Full Text Article

ORIGINAL RESEARCH

Houttuynia cordata-Derived Exosome-Like Nanoparticles Mitigate Colitis in Mice via Inhibition of the NLRP3 Signaling Pathway and Modulation of the Gut Microbiota

Jian-Hong Li[1,2,*], Jing Xu[1,2,*], Chen Huang[1,2], Jin-Xia Hu[1,2], Hao-Ming Xu[1,2], Xue Guo[1,2], Yan Zhang[1,2], Jing-Kui Xu[1,2], Yao Peng[3], Yong Zhang[1,2], Min-Zheng Zhu[1,2], You-Lian Zhou[1,2], Yu-Qiang Nie[1,2]

[1]Department of Gastroenterology and Hepatology, The Second Affiliated Hospital, School of Medicine, South China University of Technology, Guangzhou, Guangdong, People's Republic of China; [2]Department of Gastroenterology and Hepatology, Guangzhou First People's Hospital, South China University of Technology, Guangzhou, Guangdong, People's Republic of China; [3]Department of Gastroenterology and Hepatology, Shenzhen General Hospital, Shenzhen, People's Republic of China

*These authors contributed equally to this work

Correspondence: You-Lian Zhou; Yu-Qiang Nie, Department of Gastroenterology and Hepatology, The Second Affiliated Hospital, School of Medicine, South China University of Technology, No. 1 Panfu Road, Yuexiu District, Guangzhou, Guangdong, 510180, People's Republic of China, Tel +86-155-2111-7161; +86-136-0904-5779, Email eyyoulianzhou@scut.edu.cn; eyynieyuqiang@scut.edu.cn

Background: Plant-derived exosome-like nanoparticles (PELNs) have received widespread attention in treating ulcerative colitis (UC). However, the role of *Houttuynia cordata*-derived exosome-like nanoparticles (HELNs) in UC remains unclear. This study aims to evaluate the efficacy of HELNs in treating colitis in mice and investigate its potential mechanisms.

Methods: HELNs were isolated from *H. cordata* for characterization, and their safety and stability were evaluated. A dextran sulfate sodium (DSS)-induced colitis mouse model was utilized to assess the therapeutic potential of HELNs in UC. In vivo, imaging and flow cytometry were utilized to investigate the targeting effect of HELNs on inflamed colonic sites and their modulation of the immune environment. RNA-seq analysis and molecular docking were performed to identify potential pathways recruited by HELNs. Guided by transcriptomic findings, NLRP3$^{-/-}$ mice were used in conjunction with Western blotting, qPCR, immunofluorescence, and other techniques to verify that HELNs alleviated DSS-induced colitis by inhibiting NLRP3/NOD-like receptor signaling pathways. Lastly, the impact of HELNs on the gut microbiota was investigated through 16S rRNA sequencing.

Results: HELNs significantly reduced the severity of DSS-induced colitis in mice, alleviating colitis symptoms and histopathological damage. Furthermore, HELNs can specifically target inflamed colon tissue, regulate the immune environment, and decrease inflammation. RNA-seq analysis, coupled with the use of NLRP3$^{-/-}$ mice, demonstrated that HELNs inhibited the NLRP3/NOD-like receptor signaling pathways. Lastly, HELNs balanced the gut microbiota composition in mice with colitis, decreasing the abundance of harmful bacteria and increasing the abundance of beneficial bacteria in the intestinal tract of these mice.

Conclusion: In summary, HELNs exhibit the potential to protect the colon from DSS-induced damage by inhibiting the NLRP3/NOD-like receptor signaling pathway and modulating the gut microbiota, presenting a promising therapeutic option for the management of UC.

Keywords: *Houttuynia*-derived exosome-like nanoparticles, HELNs, NLRP3, gut microbiota, ulcerative colitis, UC

Introduction

Ulcerative colitis (UC), a prominent subtype of inflammatory bowel disease (IBD), predominantly affects the colon and rectum, presenting symptoms such as abdominal pain, diarrhea, and bloody stools. The global incidence of UC has been consistently rising,[1] posing significant health challenges and economic burdens on healthcare systems worldwide. The

Received: 28 August 2024
Accepted: 19 December 2024
Published: 27 December 2024

Graphical Abstract

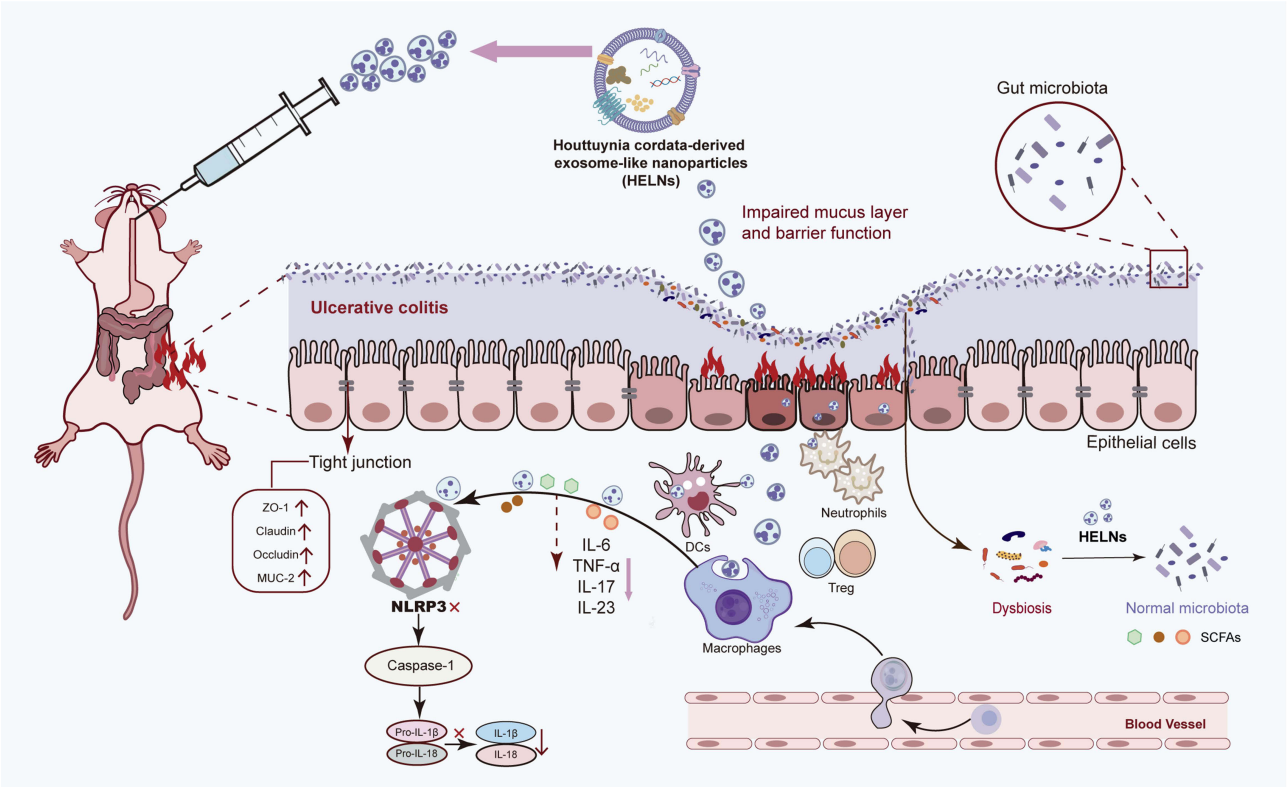

pathogenesis of UC is multifactorial, involving a complex interplay of genetic predispositions, environmental triggers, microbial dysbiosis, and dysregulated immune responses.[2] Current therapeutic strategies primarily include 5-aminosalicylic acid as the first-line treatment for inducing and maintaining remission in mild to moderate cases, whereas oral corticosteroids are reserved for moderate to severe manifestations. Furthermore, targeted therapies, including monoclonal antibodies against tumor necrosis factor (TNF), α4β7 integrin, interleukin-12 (IL-12), and IL-23 cytokines, as well as oral small-molecule agents that inhibit Janus kinases or sphingosine-1-phosphate, have been introduced to manage UC.[3–6] Despite the availability of these treatments, they are often limited by variable efficacy, potential drug dependency, the emergence of drug resistance, and adverse effects such as allergic reactions, gastrointestinal disturbances, and increased malignancy risks.[7–9] Consequently, the development of innovative therapeutic agents that are not only safe and efficient but also cost-effective is urgently needed, particularly those that can target inflamed colonic regions to reduce systemic exposure and mitigate associated side effects.

Recent advancements in nanotechnology have sparked significant interest in using nanoparticle (NP) drug carriers for the treatment of IBD. These NPs offer substantial therapeutic advantages owing to their unique properties, including diminutive size, low immunogenicity, versatile surface modification capabilities, and targeted delivery potential.[10–13] Various synthetic NP therapeutics (NTs), such as transferosomes, liposomes, dendrimers, mesoporous silica, solid lipid NPs, microspheres, and mammalian extracellular vesicles (EVs) have been developed for colon-specific drug delivery.[14–16] These NTs primarily encapsulate unstable compounds to enhance their solubility, stability, and effective concentration.[17–19] However, the complexity and cost of preparing synthetic NPs, along with challenges associated with scalability, stability, consistency, and potential biocompatibility and toxicity concerns, limit their clinical applicability. In contrast, plant-derived exosome-like nanoparticles (PDENs) sourced from edible plants, including grapefruit,[20] mulberry bark,[21] and ginger,[22] demonstrate low immunogenicity, high biocompatibility and bioavailability, and ease of preparation, making them superior

alternatives to traditional synthetic NPs. Notably, PDENs can spontaneously secrete EVs that carry therapeutic biomolecules, exerting anti-inflammatory effects in the gastrointestinal tract and addressing the limitations of synthetic NTs. The unique characteristics of PDENs underscore their potential for clinical utilization in managing various diseases, particularly UC.

Houttuynia cordata, a globally distributed medicinal and food homologous plant, is renowned for its rich nutrient profile and functional components, particularly its high concentrations of volatile oils and flavonoids. Historically utilized as both an edible vegetable and a potent traditional Chinese medicine.[23] *H. cordata* has gained recognition in recent years as a health-promoting agent with notable pharmacological effects, including anti-inflammatory, antibacterial, and antiviral properties.[24–26] Recent studies have demonstrated that *H. cordata* effectively alleviates colitis in murine models by inhibiting macrophage infiltration, suppressing the expression of proinflammatory cytokines (such as TNF-α, IL-1β, and IL-6) and proteins (Toll-like receptor 4 [TLR4] and nuclear factor-kappa B [NF-κB]), and restoring the functional imbalance between T helper 17 (Th17) cells and regulatory T (Treg) cells.[27–29] The active constituents of H. cordata, including polysaccharides, flavonoids, and compound decoctions have been explored for their therapeutic potential of modulating the expression of the Toll-like receptor 4 in IBD, highlighting their promising potential as a novel therapeutic strategy.[28,30,31] This study is the first to successfully isolate and purify native, exosome-mimicking NPs derived from *H. cordata*. This was achieved by employing a synergistic approach that combines differential and density gradient centrifugation techniques. The primary objective of this study was to explore the therapeutic potential of these NPs, referred to as *Houttuynia*-derived exosome-like nanoparticles (HELNs), in the prevention and treatment of IBD. The advantages of this approach lie in its ability to yield highly purified NPs that closely resemble natural exosomes, thereby enhancing their biocompatibility and therapeutic efficacy. Our investigation revealed that HELNs effectively alleviate colitis by inhibiting the expression of pro-inflammatory cytokines while simultaneously upregulating the secretion of anti-inflammatory cytokines and barrier-protective factors. Notably, upon oral administration, HELNs demonstrate a remarkable capacity for selective targeting of inflammatory sites in mouse models of dextran sulfate sodium (DSS)-induced UC. This targeting is facilitated through the uptake of HELNs by intestinal immune cells and epithelial populations, which subsequently modulate the immune microenvironment. Ultimately, HELNs exert a protective effect against DSS-induced colitis in mice by inhibiting the NOD-like receptor family, pyrin domain-containing 3 (NLRP3)/receptors that contain nucleotide-binding oligomerization domain (NOD)-like receptor signaling pathway, thereby restoring intestinal homeostasis and ameliorating dysbiosis.

Materials and Methods

Isolation, Purification, and Characterization of HELNs

Isolation and Purification of HELNs: Fresh *H. cordata* rhizomes were thoroughly cleaned, drained of surface moisture, cut into small pieces, and homogenized. The resulting filtrate, obtained after discarding the filter residue, was mixed with an equal volume of phosphate-buffered saline (PBS). Large particulate debris and plant fibers were removed via low-speed centrifugation (3500 ×*g*, 30 min), and the supernatant was retained. Subsequently, medium-speed centrifugation (10000 ×*g*, 60 min) was performed to eliminate larger fragments and intact organelles, and the supernatant was retained. Finally, ultrahigh-speed centrifugation (150000 ×*g*, 90 min) was employed to isolate the pellet containing HELNs. The pellet was resuspended in sterile PBS to obtain a suspension, which was then layered onto a sucrose gradient (60wt%, 45wt%, and 30wt% in 20 mm Tris-Cl, pH 7.2) in a centrifuge tube using a SW41 rotor (Beckman Coulter, Fullerton, CA, USA).[32–34] Ultracentrifugation (150000 ×g) was performed for 90 min at 4°C, and the visible band at the 30–45% sucrose interface was collected. This fraction was washed three times by adding sterile PBS and conducting ultracentrifugation (150000 ×*g*) for 90 min at 4°C to remove the sucrose solution. The separated and purified HELNs pellet was resuspended in PBS. Using the Exosome Protein Quantification Assay Kit (manufactured by Nanjing Yiwei Jianhua Biotechnology Co., Ltd., with a product number of EV02-04-01), the concentration of HELNs obtained was quantified based on protein concentration.

Characterization of HELNs: The presence of *H. cordata*-derived EVs was validated through transmission electron microscopy (TEM). Nanoparticle tracking analysis (NTA; Nanocoulter, RESUNTECH, China) was performed, according

to the manufacturer's instructions, to analyze HELN samples and determine the size and concentration distribution range of H. cordata-derived exosome-like NPs. The ζ-potential of HELNs was measured using a dynamic light scattering (DLS) system from Malvern Instruments (Malvern, UK). In Vitro Stability Test: Simulated gastric fluid (SGF) was prepared by dissolving 2.0 g of NaCl and 3.2 g of pepsin (P816235, Macklin) in approximately 1000 mL of water with 7.0 mL of hydrochloric acid, and adjusting the pH to 1.2. One milliliter of SGF was mixed with HELNs, which were initially suspended in PBS. This mixture was then incubated at 37°C for 3 hours to evaluate the stability of HELNs in the gastric environment. Following the gastric incubation, a separate batch of HELNs suspended in PBS was used for the intestinal stability test. Simulated intestinal fluid (SIF) was prepared by dissolving 6.8 g of potassium dihydrogen phosphate (P815662, Macklin) in 500 mL of water, adjusting the pH to 6.8 with a 0.1 M sodium hydroxide solution, and mixing it with a sufficient amount of water to dissolve 10 g of pancreatin (P916050, Macklin). The solution was subsequently diluted to 1000 mL. One milliliter of this SIF was mixed with the separate batch of HELNs and incubated at 37°C for 3 hours. The stability of HELNs in both SGF and SIF was evaluated by measuring their particle size and ζ-potential after the respective incubation periods.

Targeted Metabolomics Analysis

The samples of HELNs were evaluated by targeted quantitative metabolomics using the Q300TM system (Metabo-Profile, China). Furthermore, the Q300TM can measure over 300 small molecule metabolites, and quantitative analysis is performed using ultra-high performance liquid chromatography coupled to the tandem mass spectrometry UPLC-MS/MS system provided by Novogene (Beijing) Co., Ltd. Calibration was performed using isotopic internal standards, and more than 300 standard reference materials were used to quantify metabolite concentrations within different linear ranges. Microtiter plate detection, with MRM multi-channel simultaneous acquisition of retention time and ion pair information, ensures accurate identification of metabolites. These metabolites were annotated using the Kyoto Encyclopedia of Genes and Genomes (KEGG) database (http://www.genome.jp/kegg/), the HMDB (http://www.hmdb.ca/), and the LipidMaps database (http://www.lipidmaps.org/).

Cell Culture

The RAW 264.7, NCM460, SW480, and HT29 cell lines, obtained from American Type Culture Collection (ATCC) (Manassas, VA) were used in our experiments and cultured in high-glucose DMEM. To prepare the complete medium, we added 10% v/v heat-inactivated fetal bovine serum (FBS) and penicillin/streptomycin at 100 U/mL to basic DMEM. All cells were maintained in culture dishes or flasks at 37°C in a humidified atmosphere containing 5% CO_2, in accordance with the predetermined experimental protocols.

Vesicle Labeling

For experimental purposes, three different dyes were utilized to label the vesicles: Celltracker CM-lipophilic carbocyanine dye DiL (40718ES50, Yeasen; Shanghai, China), DiR (HY-D1048, MCE), and DiO green fluorescent probe for cell membranes (C1038, Beyotime). Briefly, a 5 mm solution of each dye was added to 0.5 mg of HELNs (0.5 mL in PBS), and the mixture was incubated at approximately 20°C–25°C for 30 min. Subsequently, the labeled HELNs were subjected to a 100-kDa ultracentrifuge filter to remove any free dye. The resulting labeled HELNs were suspended in PBS for subsequent experiments.

In vitro Internalization of HELNs

RAW 264.7, NCM460, SW480, and HT29 cells were seeded at a density of 2×10^5 cells per well in 35 mm glass-bottom /confocal dishes (BS-20-GJM, Biosharp) and incubated overnight in a growth medium. HELNs were labeled with the lipophilic carbocyanine dye DiL (Ex: 549 nm; Em: 565 nm) at a concentration of 5 mm. Subsequently, the labeled HELNs (10 mg/mL) were incubated with the cells for 2 h. Subsequently, the cells were washed two to three times with PBS, and the cell membranes were labeled by incubating the cells with 10 mm DiO (Ex: 484 nm; Em: 501 nm) for 20 min at 4°C. Afterward, the cells were washed three times with PBS to remove unbound dye. Finally, the cell nuclei were stained by co-incubating the cells with a 4′,6-diamidino-2-phenylindo (DAPI) staining solution (C1005, Beyotime)

for 5 min. The cells were then observed and imaged using a Zeiss LSM 900 confocal microscope equipped with Zen 3.10 software.

Animal Studies

Male C57BL/6 mice, 8 weeks old and weighing 24–27g, were purchased from the Guangdong Medical Laboratory Animal Center (License No. SCXK [Guangzhou] 2022–0002). Homozygous NLRP3-deficient ($NLRP3^{-/-}$) mice were generously provided by Dr. Lianxiang Luo of Guangdong Medical University, Zhanjiang, Guangdong. The animals were acclimated for 1 week in a specific pathogen-free room, maintained on a 12-h light/dark cycle, with an ambient temperature of 24°C ± 1°C, and a humidity range of 50–70%. All animal experiments were approved by the Animal Ethics Committee of the Second Affiliated Hospital of South China University of Technology (Guangzhou First People's Hospital).

Identification of Nlrp3 Gene Knockout Mice

The obtained *Nlrp3* gene knockout mice were mated and propagated, and DNA was extracted from their offspring for electrophoresis identification. The size of the bands and the primer sequences were determined based on the location of the gene knockout. During PCR amplification, three primer sequences were added simultaneously, one of which is common to both wild-type and knockout genotypes. The knockout homozygous genotype should exhibit a band at 500 bp, the wild-type at 250 bp, and the heterozygous genotype at both 500 bp and 250 bp. As shown in Figure S3, we selected DNA from the tails of three wild-type C57BL/6 mice and the progeny to be identified for electrophoresis. The identification confirmed that all were homozygous knockout mice.

Hemolysis Reaction Test and Biological Safety Test of HELNs

To evaluate the hemolytic properties of HELNs, we centrifuged fresh mouse blood at 3000 ×*g* for 15 min to obtain blood cells. Subsequently, 1 mL of HELNs at various concentrations (25–1000 μg/mL), 1 mL of double-distilled water, and 1 mL of PBS solution were each mixed with 20 μL of blood cells. The mixtures were incubated at 37°C for 3 h, followed by centrifugation at 3000 ×*g* for 15 min. The supernatants were then transferred to a 96-well plate, and the absorbance of each sample at 542 nm was measured using a microplate reader to calculate the hemolysis rate.

To assess the biological safety of the vesicles, we randomly divided 8-week-old male C57BL/6 mice into three groups: a healthy control group, a low-concentration group of HELNs (L-HELNs, 25 mg/mL, 200 μL per mouse), and a high-concentration group of HELNs (H-HELNs, 50 mg/mL, 200 μL per mouse). Mice in the HELN treatment groups received the corresponding HELN doses via oral gavage once daily for 7 consecutive days. On day 7, the mice were euthanized via CO_2 inhalation. Colonic tissue, serum, and major organs (including the heart, liver, spleen, lungs, and kidneys) were collected for further examination.

In vivo Therapeutic Effects of HELNs on Colitis in Mice

Following 1 week of acclimatization, 8-week-old male C57BL/6 mice were randomly divided into four groups: a healthy control group, a DSS group, an L-HELNs group (25 mg/mL, 200 μL per mouse), and an H-HELNs group (50 mg/mL, 200 μL per mouse). Except for those in the healthy control group, all mice were administered 3% DSS in their drinking water continuously for 7 days to induce colitis. Mice in the DSS, L-HELNs, and H-HELNs groups received 200 μL of PBS and 200 μL of HELNs at various concentrations, respectively, through oral gavage for 1 week. Body weight and physical activity were recorded daily, and the disease activity index (DAI) was assessed based on the scores for weight loss, stool consistency, and the presence of blood in the feces. Upon completion of the experimental procedure, the mice were euthanized through CO_2 inhalation, and blood, colorectal tissue, and cecal contents were collected. The length of the colon tissue was also measured.

Based on the findings of previous experiments, 8-week-old male C57BL/6 mice were randomly assigned to three groups: (i) Control-wild type (WT), (ii) DSS-WT, and (iii) HELNs-WT. Additionally, $NLRP3^{-/-}$ male mice were randomly allocated to three groups: (a) Control-$NLRP3^{-/-}$, (b) DSS-$NLRP3^{-/-}$, and (c) HELNs-$NLRP3^{-/-}$. The concentration of HELNs administered orally to mice was 50 mg/mL, with 200ul administered to each mouse. The

therapeutic effect of HELNs on DSS-induced colitis in NLRP3$^{-/-}$ mice was evaluated using the experimental methods described in this section.

In vivo Biodistribution of Orally Administered HELNs

To investigate the differences in the in vivo biodistribution of HELNs between healthy mice and mice with DSS-induced colitis, we conducted an experiment based on the findings of previous experiments. Following 1 week of acclimatization, 8-week-old male C57BL/6 mice were randomly divided into two groups: a healthy control group and a DSS group. Mice in the DSS group were continuously administered 3% DSS in sterile water for 5 days to induce colitis. Both groups were administered a single oral dose of DiR-labeled HELNs (50 mg/mL, 200 μL per mouse). The mice were humanely euthanized at predetermined time points post-gavage (3, 6, 12, and 24 h. Colonic tissue samples and samples of crucial organs, including the heart, liver, spleen, lungs, and kidneys, were harvested. Fluorescence imaging was performed using the IVIS Spectrum Series In Vivo Imaging System (PerkinElmer, Waltham, MA, USA).

Isolation of Intestinal Epithelial Cells, Dendritic Cells, Neutrophils, and Macrophages from the Colon and Their Analysis via Flow Cytometry

As previously described,[1] intestinal epithelial cells (EpCAM$^+$ cells), dendritic cells (CD11c$^+$ cells), macrophages (CD11b$^+$F4/80$^+$ cells), and neutrophils (Gr-1$^+$ cells) were isolated. Twelve hours after the oral administration of DiO-labeled HELNs, the colon was removed from mice, with or without DSS treatment. The colon was carefully cleaned of its mesentery, opened longitudinally, and washed of feces. The colon was then cut into 0.5 cm pieces, transferred to a 50 mL centrifuge tube, and shaken at 250 rpm for 20 min in Hanks' Balanced Salt Solution (HBSS) supplemented with 5% FBS and 2 mm ethylenediaminetetraacetic acid (EDTA) at 37°C. This process was repeated once, and the cell suspension was passed through 100-μm and 40-μm filters. Finally, epithelial cells (EpCAM$^+$ cells) were collected by centrifugation at 500 ×*g* for 5 min at 4°C. For isolating dendritic cells (CD11c$^+$ cells), neutrophils (Gr-1$^+$ cells), and macrophages (CD11b$^+$F4/80$^+$ cells), the remaining tissue was washed, minced, transferred to a 50 mL conical tube, and shaken for 15 min at 37°C in HBSS supplemented with 5% FBS, collagenase type VIII (1.5 mg/mL; Sigma), and DNase I (40 μg/mL; Sigma). The cell suspension was collected, passed through 100-μm and 40-μm filters, and sedimented by centrifugation at 500 ×*g* for 5 min at 4°C.

For flow cytometry, 100 microliters of a cell suspension containing 1×10^6 cells in Fluorescence-Activated Cell Sorting (FACS) buffer (Santa Cruz Biotechnology, Inc., Dallas, USA) were transferred to each well of a 96-well plate (Fisher 12,565,503). After blocking the cells with the FcrRIIb/CD16-2 antibody at 4°C for 10 min, we stained the cells with labeled antibodies at 4°C for 30 min. The cells were then washed twice with FACS buffer, fixed with 2% paraformaldehyde (PFA), and stored at 4°C. The following antibodies were used for analysis, all purchased from eBioscience (San Diego, CA, USA): dead BV510, anti-mouse CD45 PerCP, anti-mouse CD326 PE (EpCAM), anti-mouse CD11b APC, anti-mouse CD11c APC/Cy7, anti-mouse CD206 BV421, anti-mouse Gr-1 BV605, and anti-mouse F4/80 PE. Flow cytometry analysis was performed using the BD LSRFortessa flow cytometer (BD Biosciences), and data were analyzed using FlowJo software 7.6.5.

Biochemical Analysis

Blood was collected from the left ventricle of mice and stored in tubes without anticoagulants, allowing it to incubate at approximately 20°C–25°C for 30 min for 2–3 h. The supernatant, which constituted the mouse serum, was obtained by centrifugation at 3000 rpm for 15 min at 4°C. The levels of alanine aminotransferase (ALT), aspartate aminotransferase (AST), blood urea nitrogen (BUN), and creatinine (CR) in the serum were measured. All sera used for measurements were freshly prepared. The AST, ALT, BUN, and CR detection kits were provided by the Jiancheng Bioengineering Institute (Nanjing, China).

Disease Scoring

Disease scoring encompassed both the disease activity index (DAI) and histological damage assessment. The DAI was recorded daily using strict criteria that included weight loss, stool consistency, and gastrointestinal bleeding in mice, as detailed in Table S1. The experimental method involved histological scoring, which was conducted jointly by two experienced researchers, who rigorously followed the criteria outlined in Table S2 to evaluate images of colon tissue sections stained with hematoxylin and eosin (H&E). Immunohistochemical (IHC) staining results were evaluated and scored by two pathologists, who were blinded to the treatment, according to the previously established criteria specified in Table S3.

H&E Staining

Mouse colons and other organs were fixed in 4% PFA at room temperature for at least 24 h, followed by paraffin embedding. Then, the tissue was sectioned into 4-μm thick slices and stained with H&E following a previously described method.[35]

Cryosectioning

As previously outlined,[36] tissues were fixed and then rapidly frozen with optimal cutting temperature (OCT) embedding. Sections of 5–10 μm were cut, mounted on glass slides, stained, and examined under a microscope.

Immunofluorescence

As previously described,[37] immunofluorescence analysis (IFA) was performed to determine the presence of zonula occludens-1 (ZO-1), Occludin, and NLRP3 proteins in colonic tissue specimens.

IHC Staining

As previously outlined,[38] colon samples were subjected to IHC assessment to identify the presence of E-Cadherin protein. Quantitative evaluation was subsequently conducted according to the IHC scoring criteria outlined in Table S3.

Alcian Blue-Periodic Acid-Schiff (AB-PAS) Combined Staining

As previously described,[38] AB-PAS staining was performed to determine the number of goblet cells in colon samples.

Western Blotting (WB) Analysis

WB analysis was performed as previously described,[39] The primary antibodies used, including β-actain, NLRP3, IL-18, Caspase-1, Pro-IL-1β, and Cle-IL-1β, were purchased from Cell Signaling Technology in the United States.

RNA Sequencing (RNA-Seq) Analysis

Approximately 50 mg of circular tissue segments from the distal colon were excised from mice in both the DSS and DSS +HELNs experimental groups. These segments were rinsed with pre-cooled PBS to remove intestinal contents. Following rinsing, the segments were placed in RNase-free EP tubes and promptly stored in liquid nitrogen for preservation. Subsequently, total RNA was extracted from the colonic tissue of both groups of mice using an RNA extraction kit (FINOROP, Guangzhou, China) for further RNA-seq detection and analysis (n = 5). The RNA-seq sequencing was conducted by Guangzhou Gene Denovo Biotechnology Co., Ltd., (China). Finally, RNA-seq analysis was conducted using OmicShare tools, a free online platform for data analysis (https://www.omicshare.com/tools).

16S rRNA Gene Sequencing

Murine feces were freshly obtained and immediately immersed in liquid nitrogen for rapid freezing, followed by storage at −80°C. Microbial DNA extraction was performed employing the cetyltrimethylammonium bromide/sodium dodecyl sulfate (CTAB/SDS) protocol. The quality and quantity of the DNA were assessed through 1% agarose gel electrophoresis. The V3-V4 hypervariable region of the bacterial 16S rRNA gene was amplified via polymerase chain reaction

(PCR; Bio-Rad) using primers 338Fv (5′-ACTCCTACGGGAGGCAGCAG-3′) and 806R (5′-GGACTACHVGGGTWTCTAAT-3′). The PCR products were purified and sequenced using the OmicShare platform (Guangzhou Gene Denovo Biotechnology Co., Ltd., China). All valid reads were clustered into operational taxonomic units (OTUs) with a similarity threshold of 97%. Using the OmicShare tools, a complimentary web-based platform specializing in data analytics (accessible at https://www.omicshare.com/tools), we conducted 16S rRNA gene sequencing.

Molecular Docking

The two-dimensional molecular structures of schaftoside, isoquercitrin, procyanidin B2, tricetin-O-hexoside, luteolin, glutamine, trigonelline, and diosgenin (with their respective IDs listed in Table S4) were downloaded from the PubChem database (https://pubchem.ncbi.nlm.nih.gov). These structures were optimized for optimal conformations using Chem3D 19.0. Subsequently, the hydrogen atoms and charges were processed with AutoDock Tools to obtain the initial structures for docking.

Additionally, the protein structure of NLRP3 (PDB: 8WSM,[40] determined by X-ray diffraction) was obtained from the Protein Data Bank (https://www.rcsb.org). Preprocessing with PyMOL was performed to remove the original ligands and water molecules. AutoDock Tools were then used to process the hydrogen atoms and charges, providing the initial structure for docking.

Next, the docking positions and ranges were validated (Table S4), and molecular docking was performed using AutoDock Vina. Finally, the docking results were visualized with PyMOL to identify the binding sites, and the binding mechanisms were analyzed using LIGPLOT v2.2.4.

Real-Time Quantitative Polymerase Chain Reaction (RT-qPCR) Analysis

Colonic tissue RNA was isolated using the TRIzol reagent (Invitrogen). For reverse transcription, 1 μg of RNA was processed, and the quantification of target gene expression was achieved using the ChamQ SYBR qPCR Master Mix and the Biosystems 7500 platform (Thermo Fisher Scientific, USA). The primer sequences for IL-6, IL-1β, TNF-α, IL-18, NLRP3, Caspase-1, ZO-1, mucin-2 (MUC-2), IL-10, IL-17a, IL-23a, and Occludin are listed in Table S6. The comparative quantification of mRNA expression levels was performed following the $2^{-\Delta\Delta CT}$ methodology.

Statistical Analysis

Results are presented as the mean ± standard deviation (SD), based on three biological replicates. Statistical assessments were performed using GraphPad Prism 8.0 software (GraphPad, San Diego, CA, USA). A two-tailed Student's *t*-test was used to compare means between paired groups, while one-way and two-way analysis of variance (ANOVA) was employed for multiple group comparisons. Statistical significance was defined as $p < 0.05$.

Results

Characterization of HELNs

HELNs were isolated from the extract of *H. cordata* and purified through sucrose density gradient ultracentrifugation, as illustrated schematically in Figure 1A. Experimental results demonstrated a significant accumulation of the isolated HELNs at the 30–45% interface within the sucrose gradient (Figure 1B). The 30–45% fraction was aspirated and visualized via TEM, which revealed that HELNs were spherical or quasi-spherical vesicles with distinct membrane structures, resembling the morphological characteristics of exosome-like NPs (Figure 1C and D). Additionally, NTA indicated a size distribution ranging from 58 to 228 nm for HELNs, with an average diameter of 100 nm (Figure 1E). Zeta potential (ζ-potential) evaluations revealed that the surface of HELNs was negatively charged, measuring −10.13 mV (Figure 1G), consistent with the typical negative potential observed in plant-derived EVs.[41] Metabolomic analysis elucidated that HELNs comprised various bioactive components, predominantly flavonoids (15.63%), amino acids and their derivatives (14.15%), organic acids and their derivatives (8.82%), and lipids (8.33%) (Figure 1I).

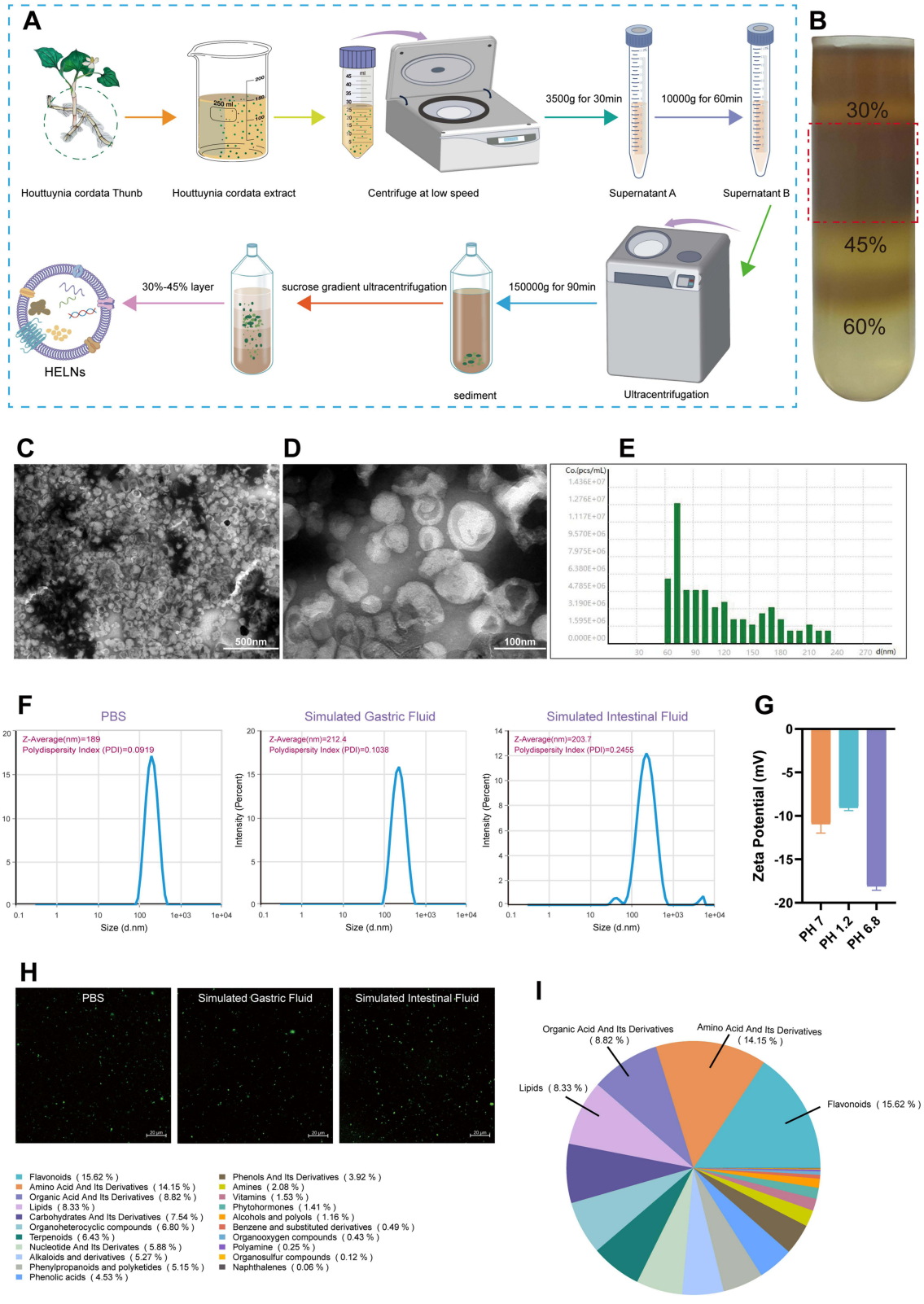

Figure 1 Characterization of HELNs. (**A**) Protocol for the extraction of HELNs, with the beaker image referenced from doi.org/10.5281/zenodo.6808870 with appropriate color modifications. (**B**) Bands formed after sucrose gradient ultracentrifugation. (**C** and **D**) TEM visualizations of HELNs displaying nanostructures; scale bars are depicted at 500 nm and 100 nm, respectively. (**E**) NTA-derived graph illustrating the particle size distribution and concentration profile of HELNs. (**F**) Particle size distribution and PDI dispersion coefficient of HELNs in different solutions. (**G**) ζ-Potential of HELNs. (**H**) Images captured using confocal microscopy after incubation with DiO-labeled HELNs in different solutions. (**I**) The results of quasi-targeted metabolomics analysis showing the proportion of metabolites of different classes in HELNs.

https://doi.org/10.2147/IJN.S493434

Resistance to the extreme conditions of the gastrointestinal tract is crucial for the efficacy of oral HELNs in treating colitis. To assess the stability of HELNs in the digestive tract, they were immersed in aqueous solutions simulating gastric and intestinal environments and subsequently analyzed for changes in ζ-potential and particle size. In the SGF, HELNs exhibited an average particle size of 212.4 nm and a decrease in negative charge. In contrast, in the SIF, HELNs exhibited an average size of 203.7 nm and an increase in negative charge (Figure 1F and G). Notably, following 3 h of incubation with PBS, the polymer dispersity index (PDI) of HELNs remained below 0.3 in both gastric- and intestinal-like solutions, indicating a uniform particle size distribution with minimal heterogeneity (Figure 1F). Confocal imaging revealed that HELNs labeled with the green fluorescent probe DiO, used for cell membranes, retained their fluorescence intensity after incubation in various aqueous solutions simulating gastric and intestinal environments (Figure 1H). These results indicate that HELNs maintain their structural integrity and resist degradation throughout their passage through the digestive tract.

Biosafety of Orally Administered HELNs

Evaluating the hemolytic activity of exosome-like NPs is essential prior to their use in drug delivery, imaging, or therapy. To examine the potential of HELNs for in vivo applications and prolonged blood contact, we measured their hemolytic rate by incubating various concentrations of HELNs with blood cells, as schematically illustrated in Figure 2A. The results indicated that even at a concentration of 300 μg/mL, the hemolytic rate of HELNs remained below 5%, demonstrating excellent blood compatibility (Figure 2B).

For assessing the safety of orally administered HELNs, mice in the L-HELNs and H-HELNs groups were administered 25 and 50 mg/mL of HELNs, respectively, daily for 7 consecutive days via gavage at a volume of 200 μL per mouse. Blood serum specimens and key visceral organs—including the heart, liver, spleen, lungs, and kidneys—were harvested from these mice in addition to those in the normal control group, and their masses were measured. Compared with those in the normal group, the levels of ALT, AST, BUN, and CR in the serum of mice in the L-HELNs and H-HELNs groups remained within normal ranges, with no significant abnormalities observed (Figure 2C). The ratios of vital organ weights to body weights in the L-HELN and H-HELN treatment groups were comparable with those in the control group (Figure 2D). Histological examination via H&E staining revealed no significant pathological changes or tissue damage in the HELN-treated groups (Figure 2E). These results suggest that, at the tested doses, HELNs do not induce significant hemolysis, hepatorenal toxicity, changes in organ weights, or tissue damage.

Oral Administration of HELNs Can Alleviate the Symptoms and Colonic Histopathological Damage in Mice with DSS-Induced Colitis

Based on the established biological safety of both L-HELN and H-HELN treatment concentrations, mice were randomly divided into four groups: control (regular water), DSS (3% DSS water), L-HELNs (3% DSS + 25 mg/mL HELNs), and H-HELNs (3% DSS + 50 mg/mL HELNs), as shown in Figure 3A. Following oral HELN intervention, the mice with colitis exhibited reduced diarrhea, bloody stool, and weight loss, along with a lower DAI score (Figure 3D and E). Additionally, colonic shortening was mitigated (Figure 3B and C). Representative H&E-stained and AB-PAS-stained sections of the distal colon are presented in Figure 3F and G. In the control group, the colonic tissue exhibited normal histomorphology with orderly arranged epithelial cells, ample goblet cells, preserved mucosa integrity, and a discrete submucosal layer.[42] However, DSS-induced colitis in mice manifested as profound epithelial atrophy/erosion, goblet cell loss, extensive crypt depletion, pronounced inflammatory cell infiltration in the lamina propria, and submucosal thickening. Notably, HELNs significantly mitigated DSS-induced pathological damage in a dose-dependent manner, as evidenced by observable crypt glands, inflammatory infiltration confined to the lamina propria, the absence of significant mixed infiltration, reduced damaged epithelial cells, and increased goblet cells compared with the DSS group ($p < 0.0001$) (Figure 3K). Compared with the DSS group (mean histological score of 10.00), the mean histological scores in the L-HELN and H-HELN treatment groups were reduced to 5.36 and 2.73, respectively ($p < 0.001$) (Figure 3J). RT-qPCR analysis demonstrated a dose-dependent suppression of the pro-inflammatory cytokines IL-6 and TNF-α, along with an increase in the anti-inflammatory cytokine IL-10 in HELN-treated mice with colitis, relative to the DSS control

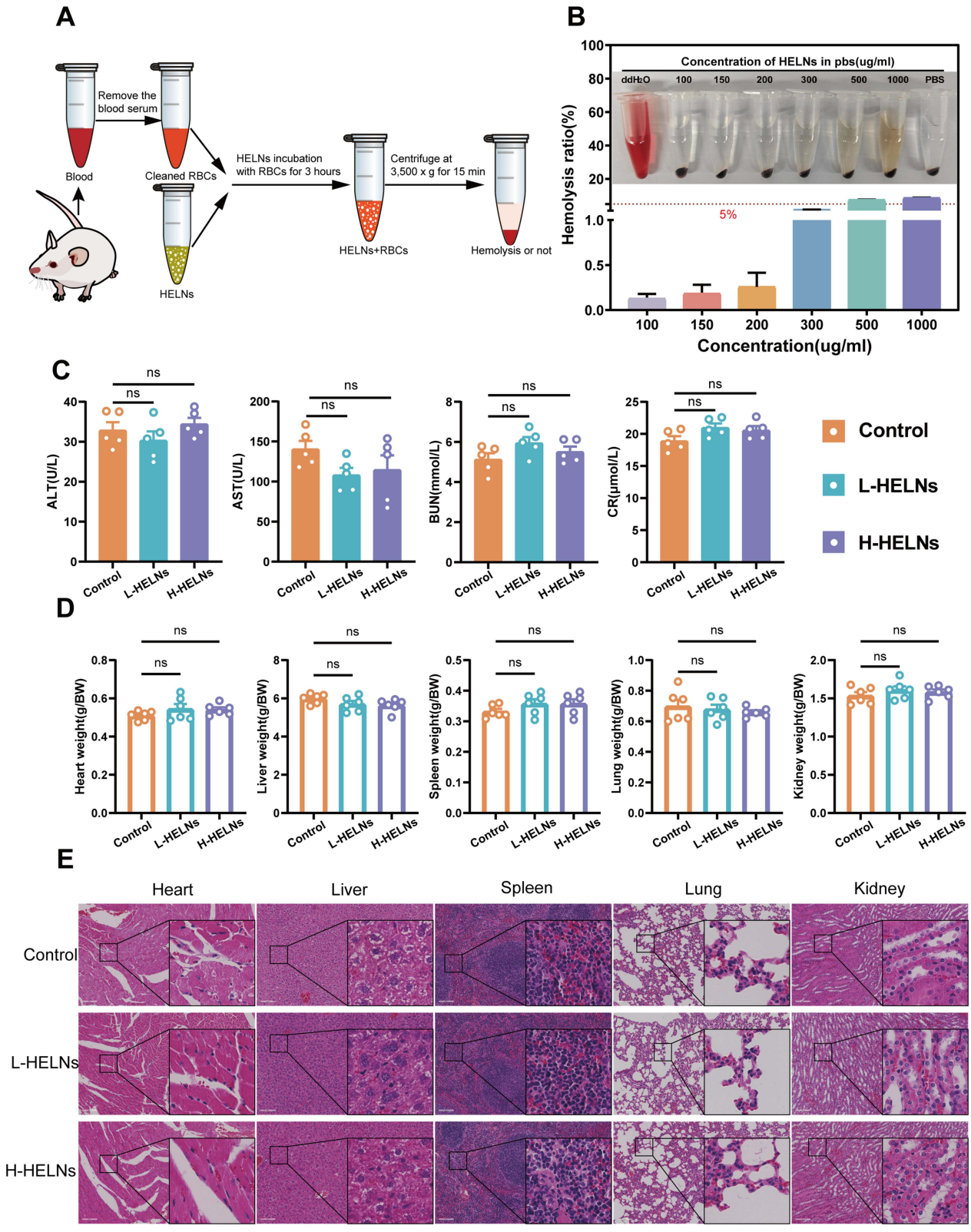

Figure 2 Biosafety of orally administered HELNs. (**A**) Experimental protocol for hemolysis detection of HELNs. The 1.5-mL Eppendorf tube in the image is adapted from doi.org/10.5281/zenodo.6808872 with color modifications; the mouse image is adapted from doi.org/10.5281/zenodo.3926533 with appropriate modifications. (**B**) Hemolysis rate of HELNs. (**C**) Liver and kidney function (n = 5). (**D**) Ratio of vital organ weight to body weight (n = 6); ns $p > 0.5$. (**E**) H&E staining of the heart, liver, spleen, lung, and kidney in control, DSS, HELNs-L, and HELNs-H groups, analyzed histologically. Scale bar: 100 μm; ns $p > 0.5$.

https://doi.org/10.2147/IJN.S493434

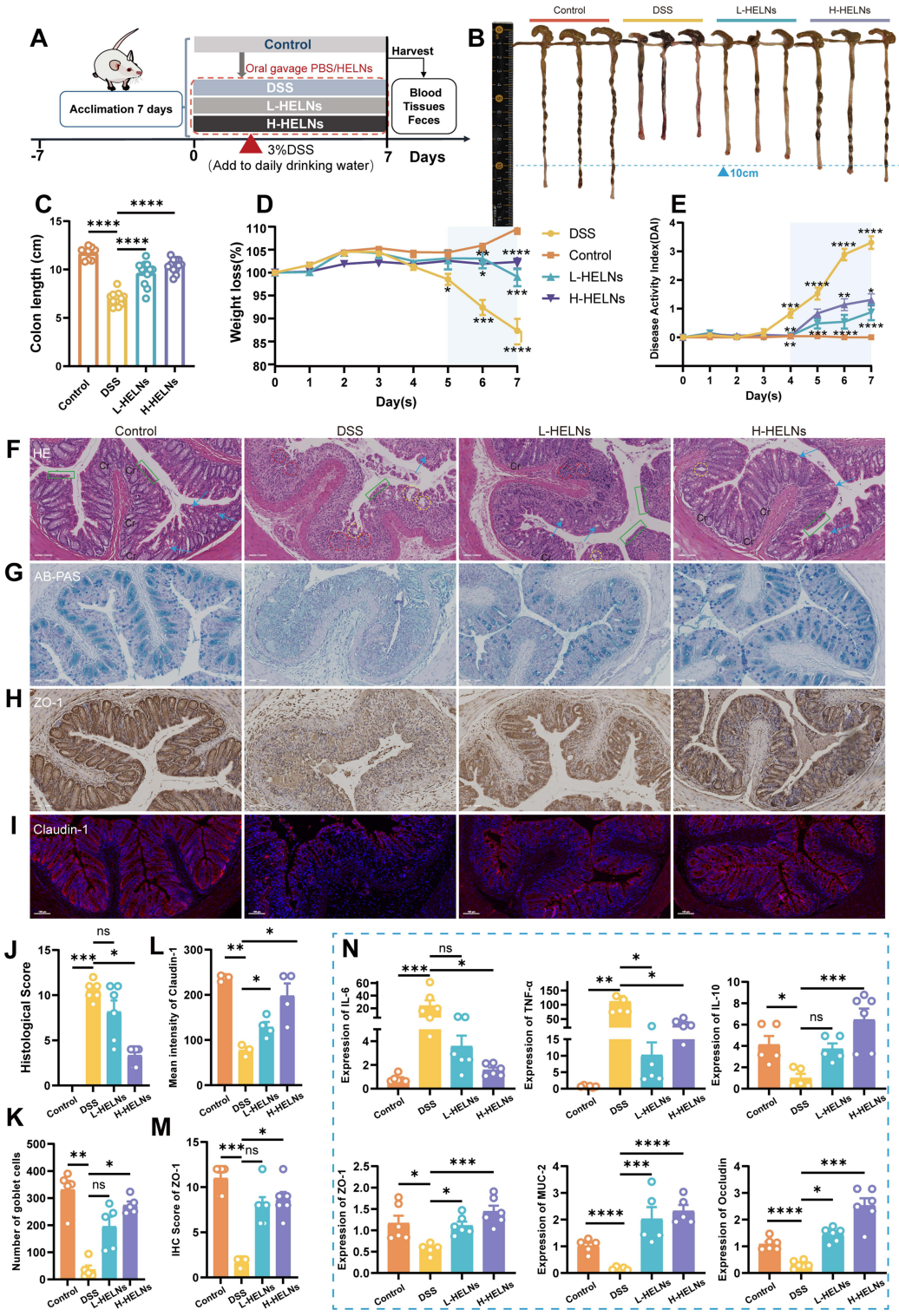

Figure 3 Oral administration of HELNs exhibited protective efficacy in mice, mitigating the onset and severity of DSS-induced colitis. (**A**) Study protocol. The mouse image is referenced from doi.org/10.5281/zenodo.3926533 with appropriate modifications. (**B** and **C**) Colon length measurements. (**D**) Variations in body mass. (**E**) DAI assessment. (**F**) Histopathological examination of intestines through H&E staining, highlighting goblet cells (blue arrows), crypt abscesses (yellow dashed lines), colonocytes (green boxes), inflammatory cell infiltration (red dashed line), and crypt architecture (Cr) annotated. (**G**) Alcian blue staining of colonic goblet cells. (**H**) IHC analysis revealed elevated ZO-1 protein levels. (**I**) Immunofluorescence analysis of Claudin-1. (**J**) Histopathological scoring of mice, assessing tissue damage across groups (n = 5). (**K**) Quantification of goblet cells in colon tissues of each group (n = 4). (**L**) Mean fluorescence intensity of Claudin-1. (**M**) IHC scores of ZO-1. (**N**) qRT-PCR analysis of IL-6, IL-10, TNF-α, ZO-1, MUC-2, and Occludin levels in colon samples from different groups of mice (n = 5–6). Scale bar: 100 μm. ns p > 0.5, *p<0.05, **p<0.01, ***p<0.001, ****p<0.0001.

group. Tight junctional complexes, which include Claudins, Occludins, junctional adhesion molecules (JAMs), and ZO proteins, regulate epithelial permeability and adhesion. These complexes are crucial structures between epithelial and endothelial cells that prevent the passage of harmful substances, pathogens, and antigens across the intestinal wall into tissues, thereby playing a pivotal role in the colonic mucosal barrier.[43] RT-qPCR results demonstrated increased relative expression levels of barrier-related factors ZO-1, MUC-2, and Occludin (Figure 3N). IHC and immunofluorescence staining showed that DSS stimulation significantly reduced ZO-1 and Claudin-1 expression, whereas HELN treatment increased the expression of these tight junction proteins (Figure 3H, I, L and M). As the HELN dose increased, the mean fluorescence density of Claudin-1 also increased, almost restoring to levels observed in the control group. Overall, the administration of HELNs in mice with DSS-induced colitis exhibits the potential to mitigate colitis symptoms, diminish colonic tissue histopathological alterations, and restore intestinal barrier integrity, thereby promoting recovery, particularly at a dose of 50 mg/mL.

Oral Administration of HELNs Enables Targeting of Inflamed Colonic Sites

In the treatment of colitis, ensuring prolonged and sufficient retention of HELNs within the colon is crucial for achieving therapeutic efficacy. To investigate their in vivo distribution, we randomly divided mice into a control group and a DSS-treated group. The DSS-treated group received 3% DSS in sterile water orally for 5 consecutive days to induce acute colitis. A single dose of DiR-labeled HELNs (50 mg/mL) was then administered orally, and abdominal fluorescence intensity was monitored using the IVIS Spectrum Series Imaging System. The results demonstrated that the fluorescence intensity peaked in both the healthy control and colitis groups 6 h post-gavage, followed by a gradual decline in both groups. Notably, 12 and 24 h after the administration of DiR-tagged HELNs orally, the DSS-treated mice (colitis model) showed higher fluorescence intensity than the healthy control group. The pattern of fluorescence intensity in ex vivo colonic tissues mirrored these changes. In the control group, abdominal fluorescence intensity significantly decreased 12 h post-gavage and was nearly absent at 24 h. In contrast, the abdominal fluorescence intensity persisted in mice with colitis 12 and 24 h post-gavage and was significantly higher than that in the control group (12 h, $p < 0.05$; 24 h, $p < 0.01$). Additionally, no significant fluorescence from DiR-labeled HELNs was observed in other organs such as the heart, liver, spleen, lungs, or kidneys (Figure 4A and B).

To validate these findings, we treated RAW264.7 cells with 100 ng/mL lipopolysaccharide (LPS) to mimic inflammation in vitro. The uptake of HELNs under normal and inflammatory conditions was then examined through confocal microscopy and flow cytometry. The results revealed a significant increase in HELN uptake by RAW264.7 cells under inflammatory conditions compared with normal conditions ($p < 0.001$) (Figure 4E–G). These results suggest that HELNs can target inflamed colonic sites and remain there longer. Endocytosis is a means for cells to acquire macromolecules and particulate substances from the extracellular environment, including phagocytosis, macropinocytosis, clathrin-mediated endocytosis, and caveolae-mediated endocytosis.[44] We employed a series of endocytosis inhibitors to investigate the mechanism of LPS-stimulated uptake of HELNs by RAW264.7 cells. The results of flow cytometry and confocal uptake experiments (as shown in Figure S1A–D) indicate that treatment of RAW264.7 cells with chlorpromazine (inhibiting clathrin-mediated endocytosis), amiloride (inhibiting macropinocytosis), and NaN_3 (which disrupts ATP production and broadly affects endocytosis) significantly decreased the uptake of HELNs, while the effect of indomethacin (inhibiting caveolin-mediated endocytosis) was less pronounced. The above results indicate that HELNs can be internalized through macropinocytosis, clathrin-dependent endocytosis, and phagocytosis.

Intestinal Epithelial Cells and Immune Cell Populations Exhibit Increased Uptake Rates of HELNs in an Inflammatory Environment

In the context of nanomedicine delivery systems, the cellular uptake process is pivotal for the effective entry of drugs into cells, thereby enabling their pharmacological actions. Based on previous data showing that HELNs target inflamed sites, we investigated the uptake of HELNs by intestinal cells under both normal and inflamed conditions. Colitis was induced in mice using 3% DSS. Colon tissues were collected from healthy mice and mice with colitis at 12 and 24 h post-administration of DiO-labeled HELNs by gavage. Frozen tissue sections were examined under a microscope. The results

 https://doi.org/10.2147/IJN.S493434

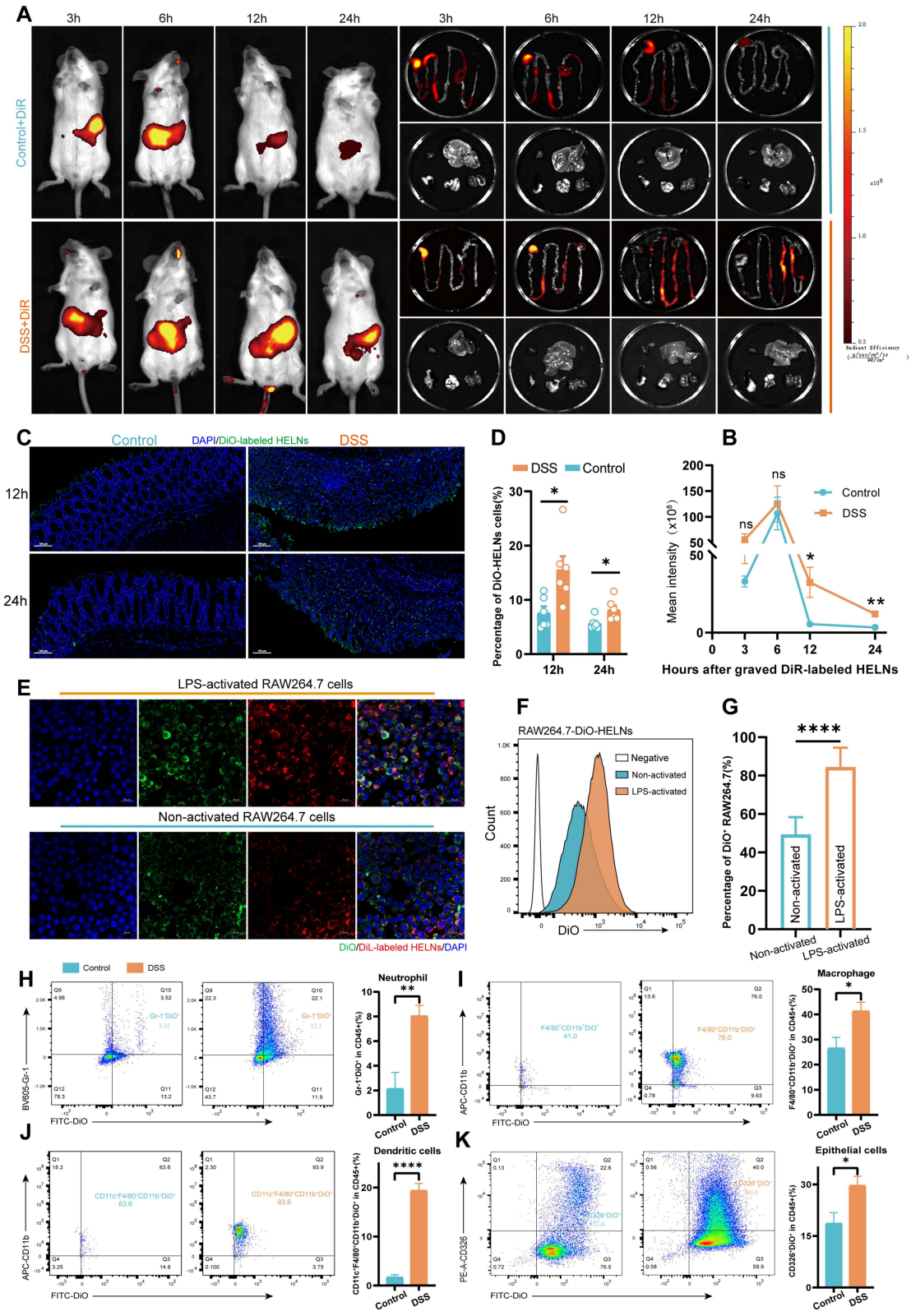

Figure 4 HELNs specifically target the site of inflammation. (**A**) GI fluorescence images display the biodistribution of DiR-HELNs at 3, 6, 12, and 24 h in both colitis and healthy mice. (**B**) Fluorescence intensity over time (n = 4). (**C** and **D**) Confocal microscopy and quantification of DiO-HELNs in DSS-colitis and healthy mice at 12 and 24 h (n = 5). Scale bar: 100 μm. (**E**) Comparison of RAW264.7 vs LPS-induced cells' phagocytosis of DiL-HELNs. Scale bar: 20 μm. (**F** and **G**) Flow cytometry detection of HELN uptake by RAW264.7 cells (n = 5). (**H**–**K**) FACS analysis of HELN uptake by intestinal cells in normal and DSS-induced colitis mice (n = 5). Significance: ns $p > 0.5$, *$p < 0.05$, **$p < 0.01$, ****$p < 0.0001$.

showed a significant increase in HELN uptake by mice with colitis compared with healthy controls at both 12 and 24 h post-administration ($p < 0.05$) (Figure 4C and D). These findings further support the specific accumulation and internalization of HELNs by intestinal cells in inflamed colons, potentially enhancing their targeted therapeutic effects against inflammation and colitis.

Colonic epithelial cells and immune cells were isolated from normal and DSS-treated mice 12 h after administering DiO-labeled HELNs. These cells were then analyzed via flow cytometry to identify the cell populations that internalized HELNs. As shown in Figure 4H, the proportions of DiO-positive neutrophils ($Gr\text{-}1^+$) were 3.52% in normal mice and 22.1% in mice with colitis. For colonic macrophages ($CD11b^+F4/80^+$), these proportions were 41% in normal mice and 76.0% in mice with colitis (Figure 4I). Dendritic cells ($CD11c^+$) exhibited proportions of 63.6% in normal mice and 93.6% in mice with colitis (Figure 4J). Lastly, colonic epithelial cells ($CD326^+$) exhibited proportions of 22.6% in normal mice and 40.0% in mice with colitis (Figure 4K). These results indicate that the primary cell populations internalizing HELNs are colonic epithelial cells ($CD326^+$), macrophages ($CD11b^+F4/80^+$), and dendritic cells ($CD11c^+$). Only a small percentage of neutrophils ($Gr\text{-}1^+$) are involved in this process. In vitro experiments were performed using HELNs labeled with the DiL dye co-cultured with RAW264.7, NCM460, SW480, and HT-29 cells. Their uptake was detected via confocal microscopy and flow cytometry. The results revealed that all four cell types could take up HELNs (Figure 5A–E). Altogether, these results demonstrate that HELNs exhibit a broad cellular affinity and uptake capacity across various intestinal cell populations, especially colonic macrophages, dendritic cells, and epithelial cells, with increased uptake under inflammatory conditions. This suggests their potential for targeted anti-inflammatory therapies against colitis.

Oral Administration of HELNs Can Modulate the Immune Microenvironment

Immune system dysfunction plays a pivotal role in the etiology of UC. It exacerbates intestinal inflammation and disrupts the balance between mucosal barrier damage and repair.[45] Given our findings that intestinal immune cells can absorb HELNs, we investigated the mechanism by which orally administered HELNs affect the immune microenvironment. Using flow cytometry, we measured the proportions of total macrophages ($F4/80^+CD11b^+$), M1 macrophages ($CD80^+$), M2 macrophages ($CD206^+$), neutrophils ($CD11b^+Gr\text{-}1^+$), and dendritic cells ($CD11c^+$) in mice with DSS-induced colitis (DSS group) and those treated with HELNs (DSS+HELNs group). The results revealed significant alterations in the composition of immune cells following HELN intervention compared with the DSS-induced model group (Figure 5F–K). Specifically, the total number of macrophages significantly decreased ($p < 0.0001$) (Figure 5G), with a notable reduction in the proportion of M1 macrophages ($p < 0.01$) (Figure 5I) and an increase in M2 macrophages ($p < 0.01$) (Figure 5H). This suggests that HELNs may inhibit pro-inflammatory M1 macrophage differentiation while promoting anti-inflammatory M2 macrophage differentiation. Additionally, the proportions of dendritic cells ($p < 0.05$) and neutrophils ($p < 0.01$) were significantly reduced following HELN treatment (Figure 5J and K). Dendritic cells are crucial for presenting antigens during immune responses, while neutrophils play a key role in acute inflammation. The diminished presence of these two cellular subsets underscores HELNs' anti-inflammatory effectiveness, achieved through the attenuation of inflammatory cell infiltration and activation, ultimately mitigating tissue injury.

Overall, these results indicate that the oral administration of HELNs modulates the immune microenvironment by decreasing the total number of macrophages, regulating macrophage polarization, and reducing the number of dendritic cells and neutrophils. This ultimately exerts an anti-inflammatory effect by diminishing the infiltration and activation of inflammatory cells.

RNA-Seq Analysis Revealed That HELNs Alleviate Colitis in Mice by Inhibiting Nlrp3 Gene Expression

RNA-seq was employed to investigate the mechanism by which HELNs protect the colons of mice with DSS-induced colitis. Transcriptomic expression levels were consistent across all 10 samples analyzed (Figure 6A). Gene expression profiling revealed significant changes between the DSS-induced colitis model and the HELN-treated group. Specifically, 199 genes were upregulated, and 326 were downregulated owing to HELN intervention (Figure 6B and C). These changes in gene expression likely contribute to the inhibition of colitis progression. Gene Ontology (GO) enrichment

 https://doi.org/10.2147/IJN.S493434

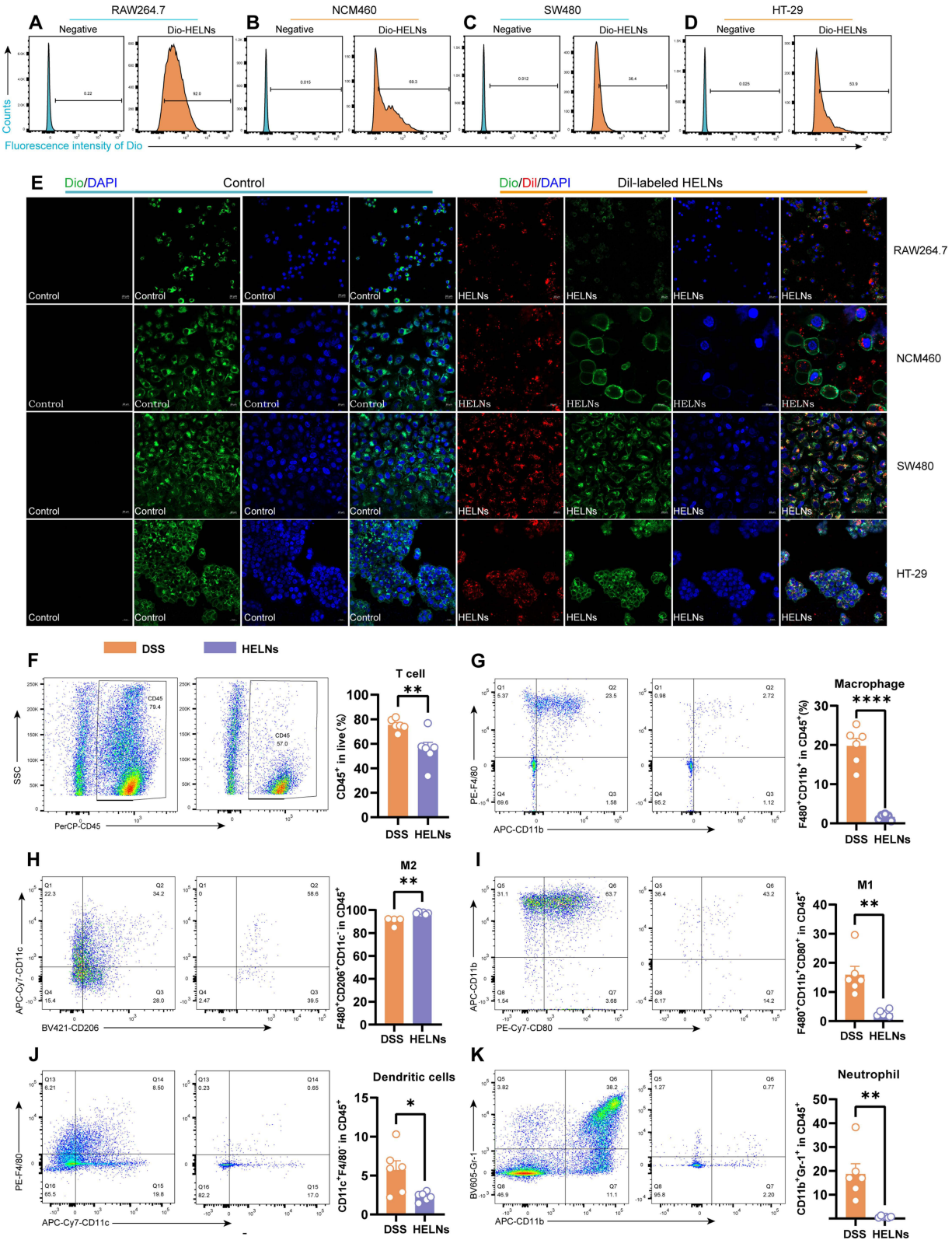

Figure 5 HELNs can modulate the immune environment. (**A**–**D**) Flow cytometry was employed to assess the cellular uptake of HELNs by RAW264.7, NCM460, SW480, and HT29 cells. (**E**) Confocal microscopy images captured the cellular uptake of HELNs by RAW264.7, NCM460, SW480, and HT29 cells. The nuclei were stained with DAPI (blue), cytoskeletal membranes were stained with DiO (green), and HELNs were labeled with the lipophilic carbocyanine dye DiL (red). Scale bar: 20 μm. (**F**–**K**) Variations in T cells, total macrophages, M1 macrophages, M2 macrophages, neutrophils, and dendritic cells were observed in mice with colitis administered with or without HELNs (n = 6). *p < 0.05, **p < 0.01, ****p < 0.0001.

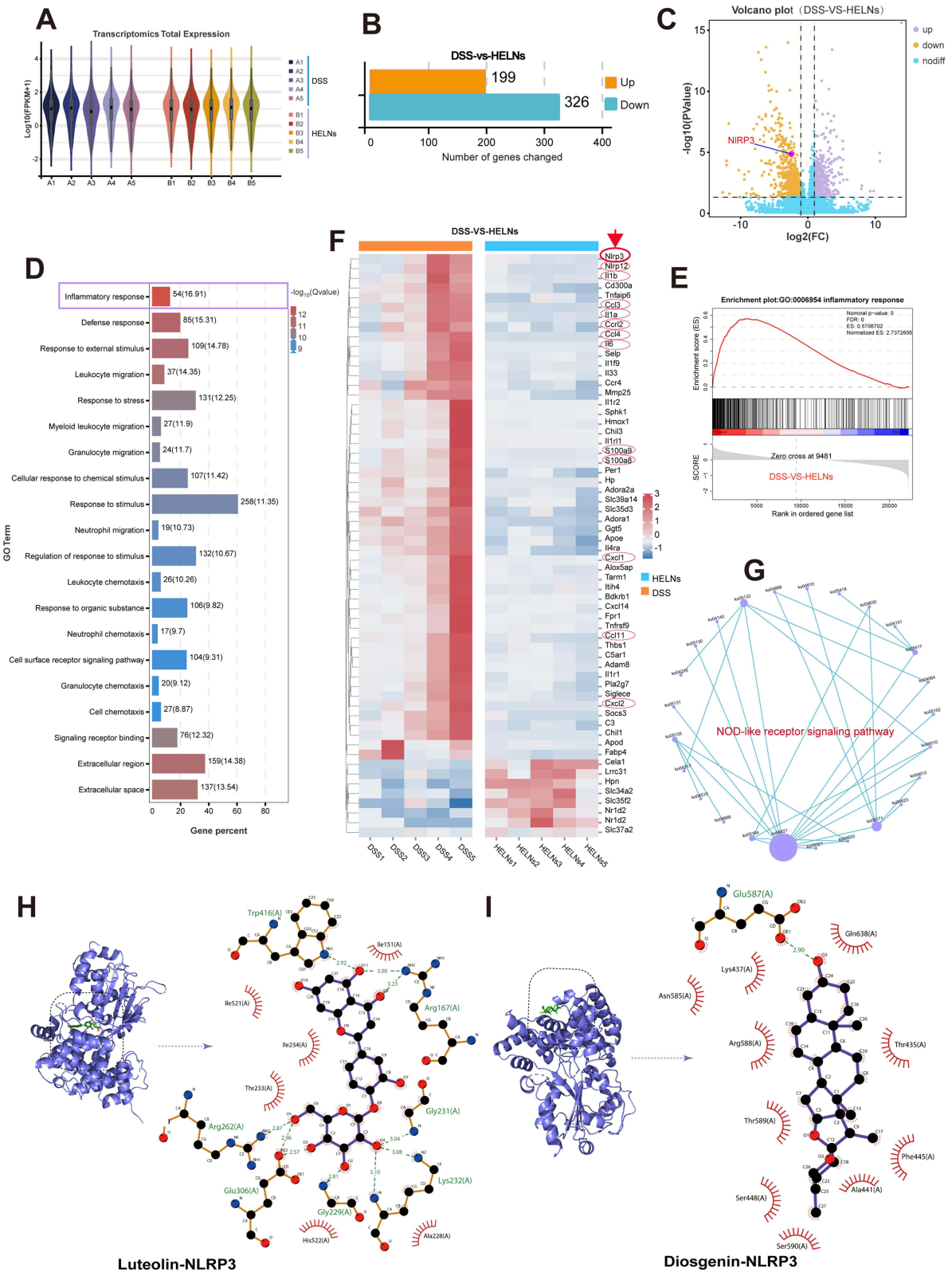

Figure 6 RNA-seq analysis showed that HELNs alleviate colitis in mice by inhibiting the NLRP3/NOD-like receptor signaling pathway. (**A**) Transcriptome expression profiles of the DSS and DSS+HELNs groups (n = 5). (**B** and **C**) Differential gene expression analysis between the two groups. (**D**) The top 20 most significantly enriched GO terms based on differential expression. (**E**) GSEA reveals significant enrichment of the inflammatory response gene set among downregulated genes. (**F**) Heatmap illustrating the expression patterns of the top 60 DEGs between the two groups. (**G**) PPI network of NLRP3 within the KEGG signaling pathways. (**H** and **I**) Molecular docking results between small molecules within HELNs and the NLRP3 protein.

https://doi.org/10.2147/IJN.S493434

analysis of these differentially expressed genes (DEGs) was performed using a significance threshold of $q < 0.05$. The results indicated that the most significantly enriched GO term in the biological process category was "inflammatory response" (GO:0006954), which encompassed 54 DEGs, accounting for 16.91% of the total DEGs (Figure 6D). These DEGs may play pivotal roles in the inflammatory response. Notably, the significant enrichment of inflammatory response-related GO terms is closely correlated with the alleviation of colitis following HELN intervention.

Gene set enrichment analysis (GSEA) was conducted, and the enrichment score plot (Figure 6E) showed a normalized enrichment score of 2.74. This indicates significant enrichment of the inflammatory response gene set (GO:0006954) among downregulated genes. Hierarchical clustering analysis was performed on the 54 DEGs (false discovery rate < 0.05) involved in the inflammatory response (GO:0006954). The clustering results were visualized using a heatmap (Figure 6F). The results revealed significant downregulation of NLRP3 in the inflammatory response following HELNs intervention. This was accompanied by the downregulation of genes such as *Nlrp12*, Ccl family members (*Ccl3, Ccl4*, and *Ccl11*), IL family members (*Il1a, Il1b*, and *Il6*), S100 family members (*S100a8* and *S100a9*), and chemokines (*Cxcl1* and *Cxcl2*). These genes exhibited similar expression patterns within the heatmap, closely associated with NLRP3 downregulation, implying their potential collaborative role with NLRP3 in regulating various stages of the inflammatory response.

To further investigate the molecular mechanisms, we constructed a protein-protein interaction (PPI) network for the KEGG pathways involving the *Nlrp3* gene (Figure 6G). The results indicated that the NOD-like receptor signaling pathway (ko04621) was the most central target. Based on the aforementioned findings, it is evident that HELNs can modulate the inflammatory environment within the intestinal mucosa by suppressing the NLRP3/NOD-like receptor signaling pathway. This modulation ultimately contributes to the mitigation of DSS-induced colitis in murine models.

HELNs Alleviate Colitis in Mice by Inhibiting the NLRP3/NOD-Like Receptor Signaling Pathway

The comprehensive RNA-seq results highlighted the importance of the NLRP3/NOD-like receptor signaling pathway. NLRP3, an inflammasome that incorporates apoptosis-associated speck-like protein (ASC), is ubiquitous in epithelial and immune cells. The overexpression, abnormal activation, polymorphisms, and gain-of-function mutations of the NLRP3 inflammasome are closely linked to IBD.[46] Metabolomic analysis of HELNs identified various bioactive molecules, with flavonoids (15.63%) and amino acids along with their derivatives (14.15%) being the major components. Other significant molecules included alkaloids and their derivatives, as well as terpenes. To investigate whether the primary bioactive molecules in HELNs function by binding to NLRP3, we performed molecular docking simulations. These simulations predicted the interactions of five major flavonoids (schaftoside, isoquercitrin, procyanidin B2, tricetin-O-hexoside, and luteolin), the most abundant amino acid derivative (glutamine), the predominant alkaloid derivative (trigonelline), and the terpenoid diosgenin with the residues of the NLRP3 protein structure (Figures 6H and I, 7A and B and S2A–D). A binding energy threshold of ≤-5.0 kJ/mol was set as the screening criterion. Binding energies of ≤-20.93 kJ/mol indicated good activity, while those of ≤-29.336 kJ/mol indicated strong binding activity.[47] The results indicated that all drug molecules could bind to the NLRP3 target. Glutamine and trigonelline exhibited weaker binding activities, while the other molecules demonstrated strong binding activities. Among them, luteolin displayed the strongest binding activity (Table S5), which may be attributed to the formation of multiple hydrogen bonds and hydrophobic interactions during the binding process between luteolin and the NLRP3 target.

The *Nlrp3* gene, part of the NOD-like receptor cascade, activates and interacts with ASC and Caspase-1 proteins to form an inflammasome complex. This process leads to the release of the proinflammatory cytokines IL-1β and IL-18, triggering immune activation and an inflammatory response. To determine if these trends were present at the mRNA level, we conducted RT-qPCR analysis to quantify the relative transcript levels of NLRP3, Caspase-1, IL-1β, and IL-18 in colonic tissues from mice. These mice were divided into three groups: control (normal water), DSS-induced colitis (3% DSS), and HELN-treated DSS groups. The results indicated a marked upregulation of NLRP3, Caspase-1, IL-1β, and IL-18 in mice with DSS-induced colitis compared with the control mice, which was substantially mitigated by HELN

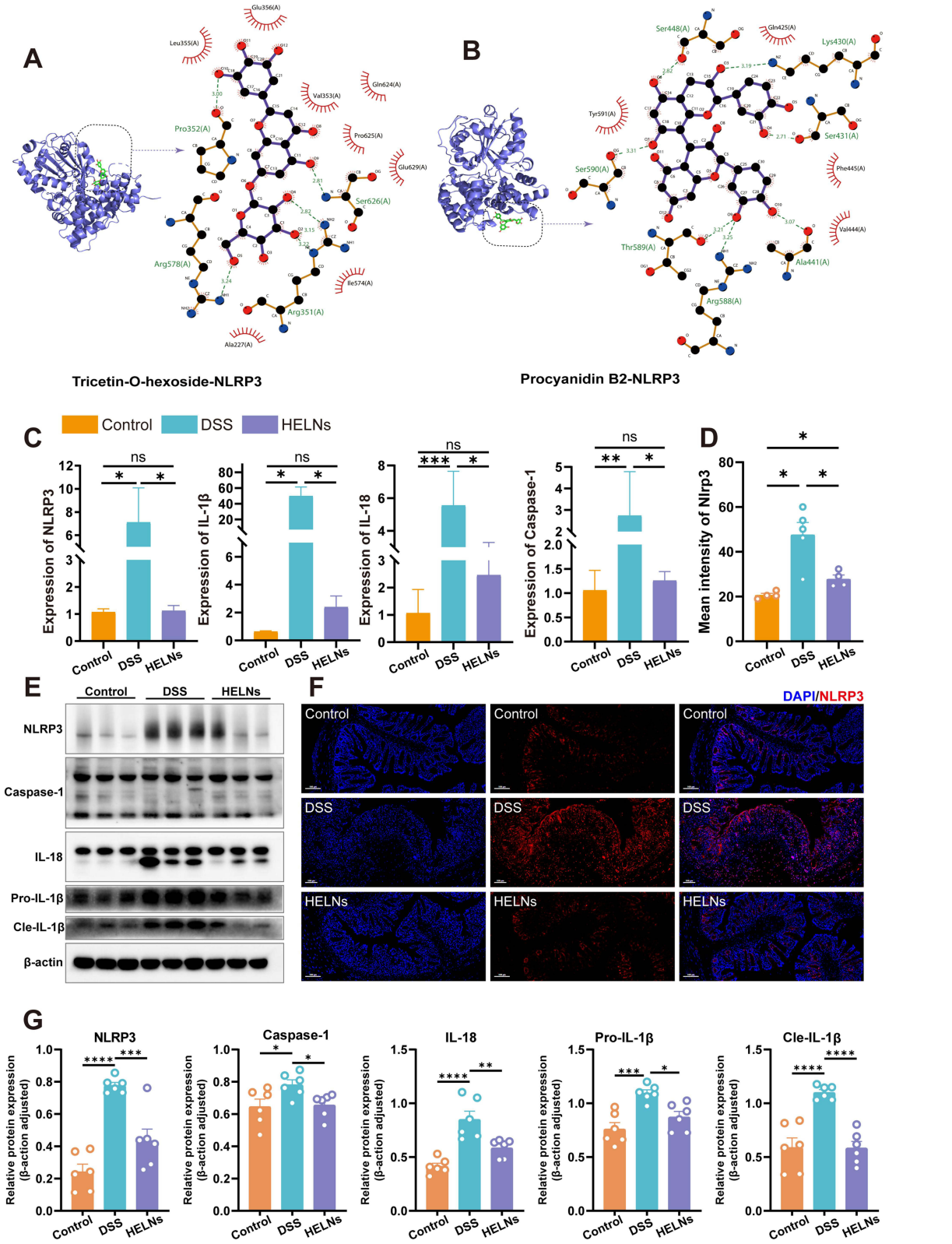

Figure 7 HELNs reduce UC symptoms in mice by suppressing the NLRP3/NOD-like receptor pathway. (**A** and **B**) Molecular docking results between small molecules within HELNs and the NLRP3 protein. (**C**) qRT-PCR detection of NLRP3, Caspase-1, IL-1β, and IL-18 levels. (**D** and **F**) Immunofluorescence images and quantitative analysis of NLRP3 expression. (**E** and **G**) The WB analysis results showed the protein expression levels of NLRP3, Caspase-1, Pro-IL-1β, Cle-IL-1β, and IL-18. ns $p > 0.5$, *$p < 0.05$, **$p < 0.01$, ***$p < 0.001$, ****$p < 0.0001$.

https://doi.org/10.2147/IJN.S493434

administration, with expression levels approximating those in non-diseased mice (Figure 7C). The WB analysis results showed that, after intervention with HELNs, the expression of NLRP3, Pro-IL-1β (precursor interleukin-1β), Cle-IL-1β (cleaved mature interleukin-1β), IL-18, and Caspase-1 proteins decreased in colitis mice (Figure 7E and G). Immunofluorescence staining revealed a higher fluorescence intensity of NLRP3 in mice with DSS-induced colitis, which was reduced to near-control levels following HELNs intervention (Figure 7D and F). These results suggest that HELNs mitigate the inflammatory milieu in DSS-induced colitis within the intestinal mucosa, potentially via suppression of the NLRP3/NOD-like receptor signaling cascade.

Knockout of the Nlrp3 Gene Significantly Augments the Therapeutic Efficacy of HELNs in Mitigating DSS-Induced Colitis in Murine Models

To elucidate the Nlrp3 gene's contribution to HELNs' actions, we examined the protective effects of HELNs in both WT and NLRP3-/- mice, as shown in Figure 8A. After 7 days of exposure to 3% DSS, the mice manifested prominent clinical features akin to UC in humans, notably substantial weight reduction, diarrhea, and hematochezia. The oral administration of HELNs reduced colonic inflammation in both WT and NLRP3$^{-/-}$ mice. Notably, NLRP3$^{-/-}$ mice showed greater improvements than WT mice. These improvements included reduced colon shortening ($p < 0.01$) (Figure 8B and C), less severe diarrhea, bloody stools, weight loss ($p < 0.01$), and lower DAI scores ($p < 0.05$) (Figure 8D and E). Notably, our study found that both HELN-treated WT mice and DSS-challenged NLRP3$^{-/-}$ mice exhibited alleviated colitis severity compared with DSS-treated WT mice, without significant differences in weight loss, DAI, diarrhea, and hematochezia. H&E staining and histopathological scoring revealed disrupted colonic mucosal structure, loss of crypt architecture, and prominent inflammatory cell infiltration in DSS-treated WT mice, while DSS-treated NLRP3$^{-/-}$ mice exhibited milder colonic damage. The oral administration of HELNs restored colonic epithelial morphology and crypt damage caused by DSS. NLRP3$^{-/-}$ mice showed greater improvement in inflammatory pathology compared with WT mice (Figure 8G). Notably, HELN-treated WT mice with colitis and NLRP3$^{-/-}$ mice with colitis showed comparable levels of colonic damage and histopathological scores, with no significant differences (Figure 8T). Goblet cells within the colon, along with their principal secretory output, mucus, are pivotal in sustaining the immunological and biological integrity of the intestinal mucosa.[48] To highlight these cells, we employed AB-PAS staining to distinguish acidic and neutral mucins, as well as glycogen content. In DSS-treated mice, the number of colonic goblet cells in WT mice was significantly reduced, whereas NLRP3$^{-/-}$ mice retained a higher number of goblet cells. Following oral HELN treatment, goblet cells persisted in both NLRP3$^{-/-}$ and WT mice, with NLRP3$^{-/-}$ mice exhibiting more intact and abundant goblet cell morphology compared with WT mice (NLRP3$^{-/-}$ vs WT, $p < 0.05$). The goblet cell counts remained comparable between the WT mice that were administered HELNs and the DSS-treated NLRP3$^{-/-}$ mice, without any notable discrepancy (Figure 8F and H). IFA revealed higher expression of Occludin and ZO-1 in colonic epithelial cells of HELN-treated mice compared with mice with DSS-treated colitis (Figure 8I and J). RT-qPCR analysis showed higher relative levels of MUC-2, Occludin, and ZO-1 in the colonic tissue of NLRP3$^{-/-}$ mice compared with WT mice, indicating improved intestinal barrier function in NLRP3$^{-/-}$ mice (Figure 8P–S). Notably, E-cadherin, an important component of intercellular adherens junctions essential for cell polarity and tissue architecture preservation, is fundamental in maintaining epithelial cell polarity and modulating intestinal barrier permeability.[49] IHC staining revealed higher E-cadherin expression in colonic epithelial cells of HELN-treated mice compared with DSS-treated mice, with NLRP3$^{-/-}$ mice exhibiting higher expression than WT mice (Figure 8K). RT-qPCR analysis revealed that HELN intervention mitigated colitis severity in mice, particularly pronounced in NLRP3$^{-/-}$ mice, as manifested by a substantial decrease in the relative mRNA expression of proinflammatory cytokines (IL-6, TNF-α, IL-17, and IL-23) compared with DSS-treated controls, with a more potent attenuation observed in NLRP3$^{-/-}$ mice (Figure 8L–O, and S). The mRNA expression patterns of IL-23, ZO-1, and Occludin were comparable between WT mice that were administered HELNs and DSS-treated NLRP3$^{-/-}$ mice, with no noteworthy discrepancies.

Together, these results suggest that *Nlrp3* gene knockout provides protection against DSS-induced colitis, and both oral administration of HELNs and *Nlrp3* gene knockout effectively mitigate DSS-induced colitis. Moreover, *Nlrp3* gene knockout significantly enhances the alleviation of DSS-induced colitis by HELNs. Overall, these results further support

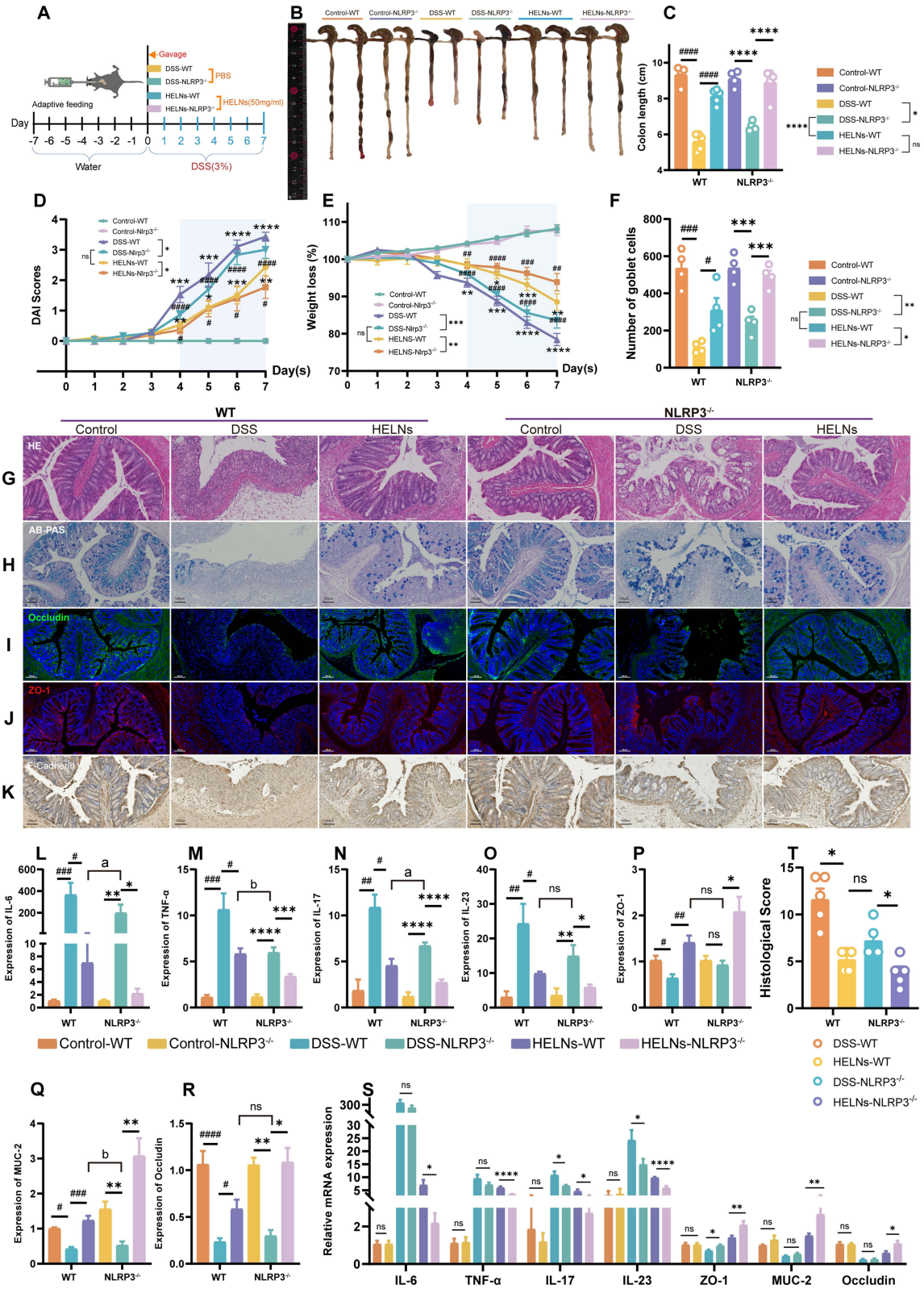

Figure 8 HELNs alleviate UC in mice by inhibiting the NLRP3/NOD-like receptor pathway. (**A**) A schematic depicting the experimental design and methodology. (**B** and **C**) Colon length measurements in each group (n = 4–5). (**D**) DAI scores for mice in each group. (**E**) Line chart showing the percentage of weight loss in mice. (**F**) Number of goblet cells in each group (n = 4). (**G**) Images of H&E-stained colon tissue. (**H**) Visualization of colonic goblet cells through Alcian blue staining. (**I**–**K**) Immunofluorescence detection of Occludin, ZO-1, and E-Cadherin protein expression. (**L**–**S**) qRT-PCR analysis of IL-6, TNF-α, IL-17, IL-23, ZO-1, MUC-2, ZO-1, and Occludin levels in colon samples from different groups of mice (n = 5–8). (**T**) Intestinal histopathological scoring based on H&E staining (n = 5). Scale bar: 100 μm. ns p > 0.5, *p<0.05, **p<0.01, ***p<0.001; ****p < 0.0001; #p<0.05, ##p<0.01, ###p<0.001, #####p<0.0001; a p<0.05, b p<0.01.

https://doi.org/10.2147/IJN.S493434

the notion that the improvement of the intestinal mucosal inflammatory environment by HELNs is associated with the inhibition of the NOD-like receptor signaling pathway and NLRP3 signaling.

Administration of HELNs Modulates Gut Dysbiosis in Mice with Colitis

The intestinal microbiome plays a crucial role in maintaining gut homeostasis, and its imbalance is a key factor in the development of UC.[50–52] To discern alterations in the gut microbiota and elucidate the potential link between the beneficial effects of HELNs on UC and the intestinal microbiome, we employed 16S rRNA sequencing. The Venn diagram analysis revealed a total of 1044 distinct OTUs across the Control, DSS, and HELNs treatment groups, derived from fecal samples. Notably, 152 OTUs were unique to the DSS group, while 175 OTUs were distinct to the HELNs group. Compared with that in mice with colitis, the OTU count significantly increased following HELN treatment (Figure 9A). We performed beta-diversity assessments using principal coordinate analysis (PCoA) and non-metric multidimensional scaling (NMDS) visualizations to measure the similarity among different microbial assemblages. The results indicated that the combined PCoA1 and PCoA2 explained more than 50% of the variance, suggesting distinct bacterial community compositions across the three groups (Figure 9B and C). Hierarchical clustering analysis supported the PCoA findings (Figure 9D). Overall, these results demonstrated significant differences in gut microbiota distribution among the groups, with HELNs specifically altering the intestinal microbiome.

To assess the impact of HELN treatment on alpha diversity indices, we analyzed the Chao1 (Figure 9E) and Shannon diversity (Figure 9F) metrics across the Control, DSS, and HELN-treated cohorts. Notably, mice with DSS-induced colitis exhibited a marginal increase in the Chao1 index compared with the controls. In contrast, HELN administration markedly elevated this index ($p < 0.05$) compared with DSS, underscoring its role in fostering intestinal microbial diversity. Analysis of the Shannon index revealed a marked decline in DSS-treated mice compared with control mice ($p < 0.05$), indicative of reduced microbial evenness. Remarkably, HELN-treated mice showed a substantial increase in the Shannon index ($p < 0.01$) compared with DSS-treated mice, suggesting HELNs' dual effect of enhancing both species richness and evenness, potentially facilitating the restoration of a healthy gut microbial ecosystem.

Utilizing the linear discriminant analysis (LDA) effect size (LEfSe) methodology, we identified significant differences among cohorts by analyzing the relative abundance of pivotal taxonomic groups, applying an LDA score cutoff of >3.5 to ensure statistical rigor (Figure 9M and N). To delve deeper into the specific changes in bacterial communities, we compared the relative abundances of the top 30 microbial communities at the phylum, family, and genus levels across the three groups, with a particular focus on those taxa exhibiting alterations in response to HELNs intervention. Figure 9G depicts the top 10 microbial communities, emphasizing *Firmicutes* and *Bacteroidetes* as the dominant phyla, accounting for more than 60% of the total sequences at the phylum level. Compared with the Control group, DSS treatment resulted in a decrease in the abundances of *Firmicutes* and *Actinobacteria*, alongside an increase in *Bacteroidota* and *Proteobacteria* (Figure S4A). Firmicutes, a crucial component of the gut microbiome, collaborate with other phyla, such as *Bacteroidetes*, to maintain intestinal microecological balance. In patients with UC, a reduction in the quantity and diversity of *Firmicutes* has been observed, potentially linked to the pathogenesis and disease progression of UC.[53] Notably, HELN administration significantly increased the relative abundances of *Firmicutes* ($p < 0.0001$) and *Actinobacteriota* ($p < 0.05$) while decreasing *Bacteroidota* ($p < 0.0001$) compared with the DSS-induced colitis group (Figure 9G and I).

At the family level, as shown in Figure 9J, DSS induction led to a significant decrease in the abundances of *Lactobacillaceae* (DSS vs Control: $p < 0.001$) and *Eggerthellaceae* (DSS vs Control: $p < 0.01$), along with a marked increase in *Bacteroidaceae* (DSS vs Control: $p < 0.0001$). Conversely, these trends were reversed following HELN treatment. Furthermore, as depicted in Figure S4B, the abundance of the beneficial genus *Oscillospiraceae* significantly increased (HELNs vs DSS: $p < 0.05$) at the family level.

At the genus level, as shown in Figure 9H, DSS treatment notably increased the relative abundances of *Escherichia-Shigella, Bacteroides*, and the *Lachnospiraceae NK4A136* genus. In contrast, the abundances of *Lactobacillus, Desulfovibrio, Alistipes*, and *Enterorhabdus* were reduced compared with the Control group. However, HELN administration notably enhanced the abundances of beneficial genera such as *Lactobacillus, Odoribacter* (Figure S4E), *Enterorhabdus*, and *Solibacillus*, while reducing those of harmful genera including *Escherichia-Shigella,*

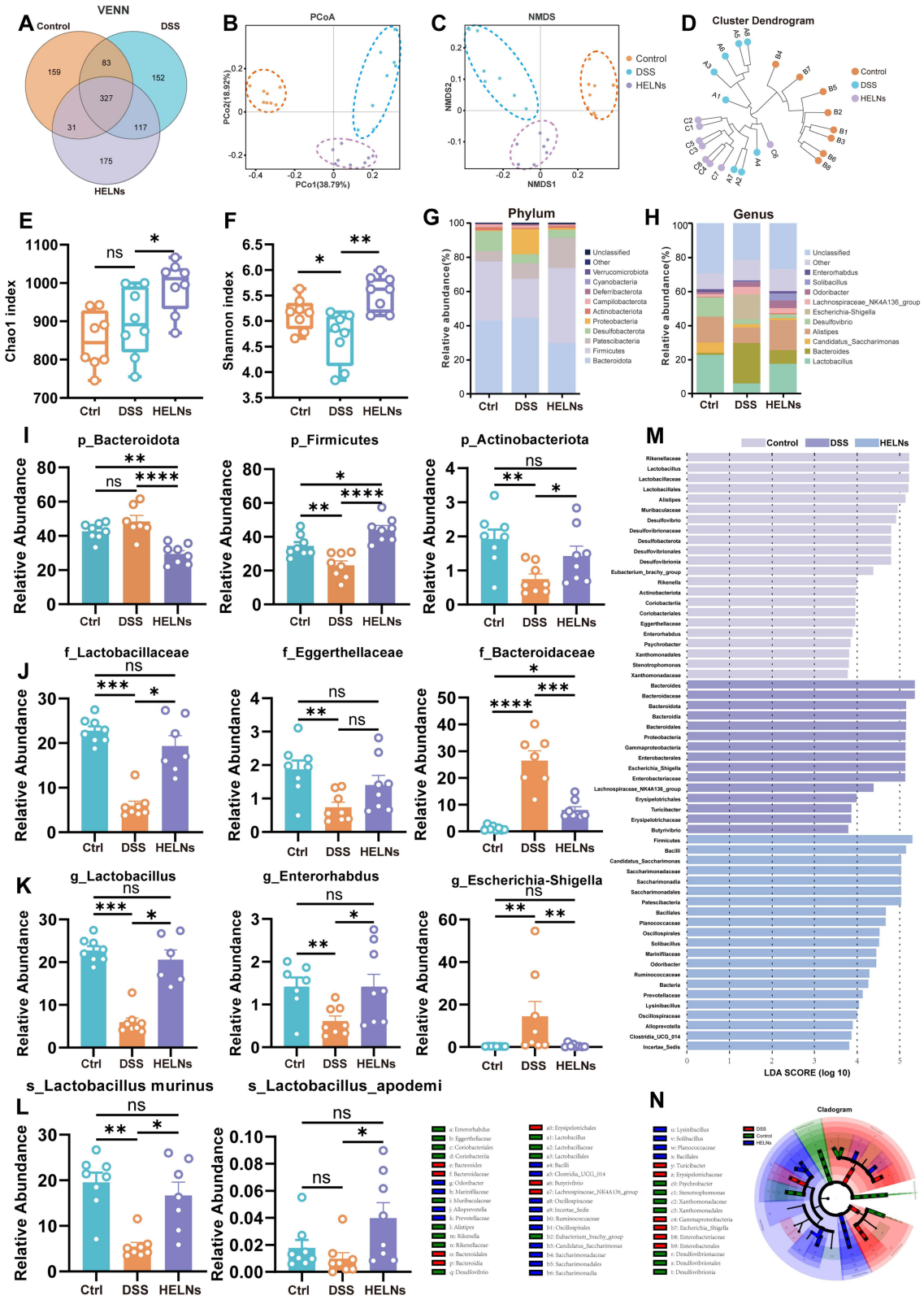

Figure 9 HELNs alter the diversity of gut microbiota in mouse models of colitis. (**A**) Venn diagram showing the overlap of OTUs identified in the gut microbiota among the four groups. (**B**) PCoA. (**C**) NMDS. (**D**) Hierarchical clustering of fecal microbiota from the three groups of mice. The Chao1 (**E**) and Shannon indices (**F**) of the fecal microbiota. (**G**) Phylum-level distribution of fecal microbiota. (**H**) Genus-level distribution of fecal microbiota. (**I**) Selected bacteria at the phylum level (n = 7–8). (**J**) Selected bacteria at the family level (n = 8). (**K**) Selected bacteria at the genus level (n = 7–8). (**L**) Selected bacteria at the species level (n = 7–8). (**M** and **N**) Microbial biomarkers in the control, DSS, and HELNs groups, with LDA score and LEfSe. ns p > 0.5, *p<0.05, **p<0.01, ***p<0.001, ****p<0.0001.

https://doi.org/10.2147/IJN.S493434

Candidatus_Saccharimonas, and *Helicobacter* (Figure S4F). Research indicates that probiotics in the gut can mitigate UC manifestations by fermenting dietary fibers, yielding short-chain fatty acids (SCFAs) such as acetate, propionic acid, and butyric acid, which reduce intestinal inflammation.[54] Consequently, we focused on the genus-level relative prevalence of bacteria capable of SCFA production. As illustrated in Figure 9K and L, HELN intervention significantly increased the abundances of SCFA-producing *Lactobacillus* (HELNs vs DSS: $p < 0.05$), *Enterorhabdus* (HELNs vs DSS: $p < 0.05$), *Solibacillus* (HELNs vs DSS: $p < 0.01$) (Figure S4C), and *Odoribacter* (HELNs vs DSS: $p < 0.01$) (Figure S4E), with a slight increase observed in *Parvibacter* (Figure S4D). Additionally, notable increases were observed in the beneficial species *Lactobacillus murinus* and *Lactobacillus apodemi* at the species level (HELNs vs DSS: $p < 0.05$) (Figure 9L). These results suggest that HELN intervention enhances gut microbiota diversity, modulates the structure of DSS-induced gut microbiota in mice, reduces harmful bacteria, and restores the abundance of dominant bacteria to achieve a new balance in the intestinal microenvironment.

Discussion

PDENs represent a novel class of nanocarriers naturally enriched with bioactive lipids, proteins, RNA, and other pharmacologically active molecules. These nanovesicles play a crucial role in modulating gene transcription and metabolic processes in target cells through the release and sequestration of diverse bioactive compounds, thereby influencing cellular functionalities.[55] Their unique morphological and compositional characteristics not only enhance their therapeutic potential but also mitigate the toxic side effects commonly associated with synthetic nanomaterials, positioning PDENs as advantageous natural alternatives.[56] Among the various diseases that could benefit from PDENs, UC stands out owing to its complex pathophysiology and the need for effective therapeutic strategies. Despite the promising attributes of PDENs, the exploration of their application in UC remains largely uncharted, highlighting a significant gap in current research that warrants further investigation.

H. cordata, a traditional medicinal herb, has garnered attention for its potent antifungal and anti-inflammatory properties, indicating significant potential for therapeutic applications. Despite its historical use in traditional medicine, the current scientific literature remains insufficient, failing to comprehensively elucidate its pharmacological value and the scope of its applications. In this study, we successfully isolated and identified a novel population of HELNs. These NPs exhibit a nanometer scale and a negative ζ-potential, which are critical parameters influencing their biological interactions and stability. The HELNs demonstrated robust stability in simulated gastric and intestinal fluids, with a polydispersity index consistently below 0.3, indicative of a uniform particle size distribution and minimal heterogeneity. This stability suggests that HELNs can withstand the complex and harsh conditions of the human gastrointestinal tract, which is essential for their potential therapeutic efficacy. Furthermore, our in vivo experiments and red blood cell hemolysis assays validated the safety and biocompatibility of HELNs, underscoring their green and safe nature with minimal toxicological concerns. This biocompatibility is particularly relevant in the context of developing novel therapeutic strategies for UC, as it suggests that HELNs could represent a simple, versatile, and cost-effective treatment modality. Notably, to our knowledge, this study is the first to investigate the preventive and therapeutic effects of HELNs on UC, thereby filling a critical gap in the existing literature.

In this study, we investigated the therapeutic potential of HELNs in a DSS-induced colitis model. Treatment with HELNs significantly ameliorated key indicators of colonic inflammation, including weight loss, colon shortening, and bloody diarrhea. Our findings demonstrated that HELNs not only reduced the DAI score but also improved histological damage, as evidenced by H&E staining. Furthermore, HELNs exhibited a dual mechanism of action by suppressing the expression of pro-inflammatory cytokines IL-6 and TNF-α while enhancing the levels of anti-inflammatory IL-10 and key tight junction proteins, including ZO-1, MUC-2, and Occludins. These findings underscore the efficacy of HELNs in mitigating DSS-induced colonic inflammation and damage. To explore the underlying mechanisms, we explored the targeting capabilities of HELNs toward inflamed colon tissue, which revealed that their negative charge facilitates adherence to the positively charged inflamed mucosa, thereby enhancing retention at sites of colitis. Subsequent analysis, including flow cytometry and in vitro phagocytosis assays, validated the substantial internalization of HELNs by immune cells and colon epithelial cells within the inflamed tissue. This targeted delivery mechanism parallels previous findings regarding the uptake of NPs by intestinal macrophages and intestinal stem cells.[20,34] Additionally, our findings suggest

that HELNs modulate the immune environment by reducing the macrophage population, altering macrophage polarization, and decreasing dendritic cell and neutrophil infiltration, ultimately exerting an anti-inflammatory effect. Collectively, these findings indicate that HELNs specifically target inflamed sites, enhancing immune cell uptake in inflammatory conditions, and thereby contributing to the regulation of the immune environment and the alleviation of UC.

To further elucidate the mechanistic basis underlying the efficacy of HELNs, we conducted a comprehensive RNA-seq analysis. The GO enrichment analysis revealed a pronounced downregulation of the *Nlrp3* gene ($p < 0.05$), while the KEGG pathway analysis identified the enrichment of several inflammatory pathways, particularly the NOD-like receptor signaling pathway, in HELN-administered mice with colitis. NLRP3, a critical component of the NOD-like receptor signaling pathway, plays a vital role in maintaining intestinal homeostasis.[57] Dysregulated activation of NLRP3 is closely associated with the disruption of the intestinal barrier and the exacerbation of UC.[46,58] Our findings align with those of previous studies that indicated increased NLRP3 expression in DSS-induced colitis models and in colon tissues of patients with IBD.[59] Strikingly, intervention with HELNs not only reversed the elevated NLRP3 expression but also resulted in a reduction of NLRP3-mediated proinflammatory cytokines, including IL-1β, TNF-α, and IL-18. These observations highlight the potential of HELNs to mitigate colitis in mice by inhibiting NLRP3 activation and the subsequent production of proinflammatory cytokines within downstream signaling cascades.

We further utilized NLRP3$^{-/-}$ mice to investigate the role of the NLRP3 inflammasome in the pathogenesis of DSS-induced colitis and to evaluate the therapeutic potential of HELNs in this context. Our findings revealed that DSS +NLRP3$^{-/-}$ mice exhibited significantly milder colitis compared with their WT counterparts, indicating a critical pro-inflammatory role of the *Nlrp3* gene and its downstream signaling pathways in the inflammatory process. Furthermore, the enhanced colitis relief observed in the HELNs+NLRP3$^{-/-}$ treatment group compared with the HELNs+WT group underscores the notion that the absence of NLRP3 facilitates a more pronounced therapeutic effect of HELNs. Notably, while HELN treatment yielded beneficial outcomes in both *NLRP3* knockout and WT mice, the slightly superior relief in the latter suggests that HELNs may not only inhibit NLRP3-mediated inflammation but also engage additional inflammatory pathways associated with DSS-induced colitis. This multifaceted mechanism of action may elucidate the enhanced therapeutic efficacy of HELNs, positioning them as a promising novel intervention in the management of colitis.

The present study also investigated the modulatory effects of HELNs on the gut microbiota in the context of UC, a condition characterized by dysbiosis and inflammation. By employing 16S rRNA sequencing, we compared the intestinal microbiome profiles of mice across three groups: Control, DSS-treated (DSS+PBS), and HELN-administered DSS-treated (DSS+HELNs). Our findings demonstrated that DSS-induced colitis in mice is associated with an increase in pathogenic bacterial genera, including *Escherichia-Shigella, Staphylococcus*, and *Helicobacter*, which were significantly reduced following HELN administration. Moreover, this study highlights the potential of HELNs to restore microbial balance by decreasing the abundance of harmful bacteria while promoting the growth of beneficial SCFA-producing bacteria. Furthermore, the observed modulation of the NLRP3 inflammasome activation pathway suggests that HELNs may play a critical role in mitigating the inflammatory response associated with UC. These findings underscore the therapeutic potential of HELNs in addressing gut dysbiosis and its implications for colitis management.

Conclusion

Our findings underscore the multifaceted role of HELNs in mitigating DSS-induced colitis through mechanisms that extend beyond mere drug delivery. By enhancing the uptake of HELNs by immune cells within inflammatory environments, we demonstrate their capacity to target inflamed tissues and reshape the immune response, thereby facilitating colitis resolution. The ability of HELNs to disrupt NLRP3/NOD-like receptor signaling pathways and reduce pro-inflammatory cytokines such as IL-1β and IL-18 further highlights their therapeutic potential. Additionally, modulation of the gut microbiota, characterized by the promotion of beneficial SCFA-producing bacteria and the suppression of pathogenic LPS-producing strains, suggests a comprehensive approach to restoring microbial balance and alleviating dysbiosis. Collectively, these attributes position HELNs as not only effective therapeutic agents but also as

environmentally friendly nanocarriers, offering a promising alternative for the treatment of intestinal inflammatory conditions such as UC.

Abbreviations

IL-1β, interleukin-1 beta; TNF-α, tumor necrosis factor alpha; ZO-1, zonula occludens-1; MUC-2, mucin-2; UC, ulcerative colitis; IL-12, interleukin-12; NTs, NP therapeutics; EVs, extracellular vesicles; PDENs, plant-derived exosome-like nanoparticles; TLR4, Toll-like receptor 4; NF-κB, nuclear factor-kappa B; Th17, T helper 17; Treg, regulatory T; NOD, nucleotide-binding oligomerization domain; PBS, phosphate-buffered saline; TEM, transmission electron microscopy; DLS, dynamic light scattering; SGF, Simulated gastric fluid; SIF, Simulated intestinal fluid; FBS, fetal bovine serum; ALT, alanine aminotransferase; AST, aminotransferase; BUN, blood urea nitrogen; CR, creatinine; IHC, Immunohistochemical; DAPI, 4′,6-diamidino-2-phenylindole; ANOVA, analysis of variance; SD, standard deviation; JAMs, junctional adhesion molecules; LPS, lipopolysaccharide; PPI, protein-protein interaction; DEGs, differentially expressed genes; GSEA, Gene set enrichment analysis; LDA, linear discriminant analysis; SCFAs, short-chain fatty acids.

Data Sharing Statement

The 16S rRNA sequencing data in this study have been submitted to the Sequence Read Archive (SRA) database according to standard procedures for sharing and reuse by the global scientific research community. Specifically, these data can be retrieved and downloaded through BioProject access number PRJNA1145974, ensuring the transparency and long-term availability of the data.

Ethics Approval and Consent to Participate

The Institutional Animal Care and Use Committee of Guangzhou Medical University approved animal experiments (Experimental Animal Certificate Number: SCXK [Guangdong] 2022-0002). Additionally, all animal experimentation protocols were subject to and approved by the Animal Ethics Committee of the Second Affiliated Hospital of South China University of Technology, concurrently serving as Guangzhou First People's Hospital. In this study, the *Houttuynia cordata* used was formally identified by Professor Ye Huagu on December 9, 2022, and is preserved at the Herbarium of the South China Botanical Garden, Chinese Academy of Sciences (voucher specimen number TLDS-618), thereby ensuring the authenticity and ethical sourcing of the plant material employed in this research.

Acknowledgments

We extend our profound gratitude to Dr. Lianxiang Luo, affiliated with Guangdong Medical University in Zhanjiang, Guangdong Province, for his benevolent contribution of homozygous NLRP3-deficient ($NLRP3^{-/-}$) mice, which have been instrumental in advancing our research endeavors. Additionally, we acknowledge with appreciation the invaluable resources furnished by the website https://scidraw.io/, which served as a source of inspiration and a reference point for the depiction of mice, centrifuge tubes, and beakers in our figures, significantly enhancing the clarity and scientific rigor of our graphical representations. Moreover, we appreciate the contribution of all experimental animals to scientific research.

Funding

Grants from the National Natural Science Foundation of China (82270577, 82370552), Natural Science Foundation of Guangdong Province (2023A1515030214), and Guangzhou Key Laboratory of Digestive Diseases (2022–2023) (KY17010003) supported this work.

Disclosure

The authors declare no competing interests or conflicts of interest in this work.

References

1. Liu C, Yan X, Zhang Y, et al. Oral administration of turmeric-derived exosome-like nanovesicles with anti-inflammatory and pro-resolving bioactions for murine colitis therapy. *J Nanobiotechnol*. 2022;20(1):206. doi:10.1186/s12951-022-01421-w
2. Danese S, Fiorino G, Peyrin-Biroulet L. Positioning therapies in ulcerative colitis. *Clin Gastroenterol Hepatol*. 2020;18(6):1280–1290.e1. doi:10.1016/j.cgh.2020.01.017
3. Gros B, Kaplan GG. Ulcerative colitis in adults. *JAMA*. 2023;330(10):951. doi:10.1001/jama.2023.15389
4. Verstockt B, Vetrano S, Salas A, et al. Sphingosine 1-phosphate modulation and immune cell trafficking in inflammatory bowel disease. *Nat Rev Gastroenterol Hepatol*. 2022;19(6):351–366. doi:10.1038/s41575-021-00574-7
5. Rogler G, Singh A, Kavanaugh A, Rubin DT. Extraintestinal manifestations of inflammatory bowel disease: current concepts, treatment, and implications for disease management. *Gastroenterology*. 2021;161(4):1118–1132. doi:10.1053/j.gastro.2021.07.042
6. Verstockt B, Salas A, Sands BE, et al. IL-12 and IL-23 pathway inhibition in inflammatory bowel disease. *Nat Rev Gastroenterol Hepatol*. 2023;20(7):433–446. doi:10.1038/s41575-023-00768-1
7. Maneiro JR, Salgado E, Gomez-Reino JJ. Immunogenicity of monoclonal antibodies against tumor necrosis factor used in chronic immune-mediated inflammatory conditions. *JAMA Intern Med*. 2013;173(15):1416. doi:10.1001/jamainternmed.2013.7430
8. Gao C, Zhou Y, Chen Z, et al. Turmeric-derived nanovesicles as novel nanobiologics for targeted therapy of ulcerative colitis. *Theranostics*. 2022;12(12):5596–5614. doi:10.7150/thno.73650
9. Núñez P, Quera R, Yarur AJ. Safety of janus kinase inhibitors in inflammatory bowel diseases. *Drugs*. 2023;83(4):299–314. doi:10.1007/s40265-023-01840-5
10. Hua S, Marks E, Schneider JJ, Keely S. Advances in oral nano-delivery systems for colon targeted drug delivery in inflammatory bowel disease: selective targeting to diseased versus healthy tissue. *Nanomed Nanotechnol Biol Med*. 2015;11(5):1117–1132. doi:10.1016/j.nano.2015.02.018
11. Xiao Q, Li X, Li Y, et al. Biological drug and drug delivery-mediated immunotherapy. *Acta Pharmaceutica Sinica B*. 2021;11(4):941–960. doi:10.1016/j.apsb.2020.12.018
12. Zhu Q, Chen Z, Paul PK, Lu Y, Wu W, Qi J. Oral delivery of proteins and peptides: challenges, status quo and future perspectives. *Acta Pharmaceutica Sinica B*. 2021;11(8):2416–2448. doi:10.1016/j.apsb.2021.04.001
13. Luo R, Chang Y, Liang H, et al. Interactions between extracellular vesicles and microbiome in human diseases: new therapeutic opportunities. *iMeta*. 2023;2(2):e86. doi:10.1002/imt2.86
14. Lv Y, Ren M, Yao M, et al. Colon-specific delivery of methotrexate using hyaluronic acid modified pH-responsive nanocarrier for the therapy of colitis in mice. *Int J Pharm*. 2023;635:122741. doi:10.1016/j.ijpharm.2023.122741
15. Wang X, Yan J, Wang L, et al. Oral delivery of anti-TNF antibody shielded by natural polyphenol-mediated supramolecular assembly for inflammatory bowel disease therapy. *Theranostics*. 2020;10(23):10808–10822. doi:10.7150/thno.47601
16. Wang D, Sun M, Zhang Y, et al. Enhanced therapeutic efficacy of a novel colon-specific nanosystem loading emodin on DSS-induced experimental colitis. *Phytomedicine*. 2020;78:153293. doi:10.1016/j.phymed.2020.153293
17. Li W, Li Y, Liu Z, et al. Hierarchical structured and programmed vehicles deliver drugs locally to inflamed sites of intestine. *Biomaterials*. 2018;185:322–332. doi:10.1016/j.biomaterials.2018.09.024
18. Jin K, Luo Z, Zhang B, Pang Z. Biomimetic nanoparticles for inflammation targeting. *Acta Pharmaceutica Sinica B*. 2018;8(1):23–33. doi:10.1016/j.apsb.2017.12.002
19. Yang C, Merlin D. Nanoparticle-mediated drug delivery systems for the treatment of IBD: current perspectives. *IJN*. 2019;14:8875–8889. doi:10.2147/IJN.S210315
20. Wang B, Zhuang X, Deng ZB, et al. Targeted drug delivery to intestinal macrophages by bioactive nanovesicles released from grapefruit. *Mol Ther*. 2014;22(3):522–534. doi:10.1038/mt.2013.190
21. Sriwastva MK, Deng Z, Wang B, et al. Exosome-like nanoparticles from Mulberry bark prevent DSS-induced colitis via the AhR/COPS8 pathway. *EMBO Rep*. 2022;23(3):e53365. doi:10.15252/embr.202153365
22. Zhang M, Viennois E, Prasad M, et al. Edible ginger-derived nanoparticles: a novel therapeutic approach for the prevention and treatment of inflammatory bowel disease and colitis-associated cancer. *Biomaterials*. 2016;101:321–340. doi:10.1016/j.biomaterials.2016.06.018
23. Shingnaisui K, Dey T, Manna P, Kalita J. Therapeutic potentials of Houttuynia cordata Thunb. against inflammation and oxidative stress: a review. *J Ethnopharmacol*. 2018;220:35–43. doi:10.1016/j.jep.2018.03.038
24. Wei P, Luo Q, Hou Y, Zhao F, Li F, Meng Q. Houttuynia Cordata Thunb.: a comprehensive review of traditional applications, phytochemistry, pharmacology and safety. *Phytomedicine*. 2024;123:155195. doi:10.1016/j.phymed.2023.155195
25. Ho TY, Lo HY, Lu GL, Liao PY, Hsiang CY. Analysis of target organs of Houttuynia cordata: a study on the anti-inflammatory effect of upper respiratory system. *J Ethnopharmacol*. 2023;315:116687. doi:10.1016/j.jep.2023.116687
26. Shi C, Zhou L, Li H, et al. Intestinal microbiota metabolizing Houttuynia cordata polysaccharides in H1N1 induced pneumonia mice contributed to Th17/Treg rebalance in gut-lung axis. *Int J Biol Macromol*. 2022;221:288–302. doi:10.1016/j.ijbiomac.2022.09.015
27. Cheng T, Xu C, Wu D, et al. Sodium houttuyfonate derived from Houttuynia cordata Thunb improves intestinal malfunction via maintaining gut microflora stability in Candida albicans overgrowth aggravated ulcerative colitis. *Food Funct*. 2023;14(2):1072–1086. doi:10.1039/D2FO02369E
28. Cen L, Yi T, Hao Y, et al. Houttuynia cordata polysaccharides alleviate ulcerative colitis by restoring intestinal homeostasis. *Chinese J Nat Med*. 2022;20(12):914–924. doi:10.1016/S1875-5364(22)60220-6
29. Wang J, Dempsey E, Corr SC, Kukula-Koch W, Sasse A, Sheridan H. The Traditional Chinese Medicine Houttuynia cordata Thunb decoction alters intestinal barrier function via an EGFR dependent MAPK (ERK1/2) signalling pathway. *Phytomedicine*. 2022;105:154353. doi:10.1016/j.phymed.2022.154353
30. Lu Q, Li R, Yang Y, Zhang Y, Zhao Q, Li J. Ingredients with anti-inflammatory effect from medicine food homology plants. *Food Chem*. 2022;368:130610. doi:10.1016/j.foodchem.2021.130610
31. Direito R, Barbalho SM, Figueira ME, et al. Medicinal plants, phytochemicals and regulation of the NLRP3 inflammasome in inflammatory bowel diseases: a comprehensive review. *Metabolites*. 2023;13(6):728. doi:10.3390/metabo13060728
32. Liu X, Lou K, Zhang Y, Li C, Wei S, Feng S. Unlocking the medicinal potential of plant-derived extracellular vesicles: current progress and future perspectives. *IJN*. 2024;19:4877–4892. doi:10.2147/IJN.S463145

33. Suharta S, Barlian A, Hidajah AC, et al. Plant-derived exosome-like nanoparticles: a concise review on its extraction methods, content, bioactivities, and potential as functional food ingredient. *J Food Sci*. 2021;86(7):2838–2850. doi:10.1111/1750-3841.15787
34. Ju S, Mu J, Zhuang X, et al. Grape exosome-like nanoparticles induce intestinal stem cells and protect mice from DSS-induced colitis. *Mol Ther*. 2013;21(7):1345–1357. doi:10.1038/mt.2013.64
35. Xu J, Xu H, Guo X, et al. Pretreatment with an antibiotics cocktail enhances the protective effect of probiotics by regulating SCFA metabolism and Th1/Th2/Th17 cell immune responses. *BMC Microbiol*. 2024;24(1):91. doi:10.1186/s12866-024-03251-2
36. Giobbe GG, Crowley C, Luni C, et al. Extracellular matrix hydrogel derived from decellularized tissues enables endodermal organoid culture. *Nat Commun*. 2019;10(1):5658. doi:10.1038/s41467-019-13605-4
37. Xu H, Xu J, Yang M, et al. Epigenetic DNA methylation of Zbtb7b regulates the population of double-positive CD4+CD8+ T cells in ulcerative colitis. *J Transl Med*. 2022;20(1):289. doi:10.1186/s12967-022-03477-6
38. Ma J, Zhang J, Wang Y, et al. Modified Gegen Qinlian decoction ameliorates DSS-induced chronic colitis in mice by restoring the intestinal mucus barrier and inhibiting the activation of γδT17 cells. *Phytomedicine*. 2023;111:154660. doi:10.1016/j.phymed.2023.154660
39. Guo X, Xu J, Huang C, et al. Rapamycin extenuates experimental colitis by modulating the gut microbiota. *J Gastroenterol Hepatol*. 2023: jgh.16381. doi:10.1111/jgh.16381
40. Ohba Y, Adachi K, Furukawa T, et al. Discovery of novel NLRP3 inflammasome inhibitors composed of an oxazole scaffold bearing an acylsulfamide. *ACS Med Chem Lett*. 2023;14(12):1833–1838. doi:10.1021/acsmedchemlett.3c00433
41. Fan J, Yu H, Lu X, et al. Overlooked spherical nanoparticles exist in plant extracts: from mechanism to therapeutic applications. *ACS Appl Mater Interfaces*. 2023;15(7):8854–8871. doi:10.1021/acsami.2c19065
42. da Silva Watanabe P, Cavichioli AM, D'Arc de Lima Mendes J, et al. Colonic motility adjustments in acute and chronic DSS-induced colitis. *Life Sci*. 2023;321:121642. doi:10.1016/j.lfs.2023.121642
43. Peng J, Li H, Olaolu OA, Ibrahim S, Ibrahim S, Wang S. Natural products: a dependable source of therapeutic alternatives for inflammatory bowel disease through regulation of tight junctions. *Molecules*. 2023;28(17):6293. doi:10.3390/molecules28176293
44. Conner SD, Schmid SL. Regulated portals of entry into the cell. *Nature*. 2003;422:6927):37–44. doi:10.1038/nature01451
45. Abraham C, Medzhitov R. Interactions between the host innate immune system and microbes in inflammatory bowel disease. *Gastroenterology*. 2011;140(6):1729–1737. doi:10.1053/j.gastro.2011.02.012
46. Shao BZ, Wang SL, Pan P, et al. Targeting NLRP3 inflammasome in inflammatory bowel disease: putting out the fire of inflammation. *Inflammation*. 2019;42(4):1147–1159. doi:10.1007/s10753-019-01008-y
47. Yuan C, Wang MH, Wang F, et al. Network pharmacology and molecular docking reveal the mechanism of Scopoletin against non-small cell lung cancer. *Life Sci*. 2021;270:119105. doi:10.1016/j.lfs.2021.119105
48. van der Post S, Jabbar KS, Birchenough G, et al. Structural weakening of the colonic mucus barrier is an early event in ulcerative colitis pathogenesis. *Gut*. 2019;68(12):2142–2151. doi:10.1136/gutjnl-2018-317571
49. Lu J, Liu D, Tan Y, Deng F, Li R. M1 Macrophage exosomes MiR-21a-5p aggravates inflammatory bowel disease through decreasing E-cadherin and subsequent ILC2 activation. *J Cell Mol Med*. 2021;25(6):3041–3050. doi:10.1111/jcmm.16348
50. Yuan X, Chen B, Duan Z, et al. Depression and anxiety in patients with active ulcerative colitis: crosstalk of gut microbiota, metabolomics and proteomics. *Gut Microbes*. 2021;13(1):1987779. doi:10.1080/19490976.2021.1987779
51. Zhang C, Liu H, Sun L, et al. An overview of host-derived molecules that interact with gut microbiota. *iMeta*. 2023;2(2):e88. doi:10.1002/imt2.88
52. Wang Y, Dong Q, Hu S, et al. Decoding microbial genomes to understand their functional roles in human complex diseases. *iMeta*. 2022;1(2):e14. doi:10.1002/imt2.14
53. Manichanh C. Reduced diversity of faecal microbiota in Crohn's disease revealed by a metagenomic approach. *Gut*. 2006;55(2):205–211. doi:10.1136/gut.2005.073817
54. Xing PY, Pettersson S, Kundu P. Microbial metabolites and intestinal stem cells tune intestinal homeostasis. *Proteomics*. 2020;20(5–6):1800419. doi:10.1002/pmic.201800419
55. Logozzi M, Di Raimo R, Mizzoni D, Fais S. The potentiality of plant-derived nanovesicles in human health—a comparison with human exosomes and artificial nanoparticles. *IJMS*. 2022;23(9):4919. doi:10.3390/ijms23094919
56. Dad HA, Gu TW, Zhu AQ, Huang LQ, Peng LH. Plant exosome-like nanovesicles: emerging therapeutics and drug delivery nanoplatforms. *Mol Ther*. 2021;29(1):13–31. doi:10.1016/j.ymthe.2020.11.030
57. Liu C, Zeng Y, Wen Y, Huang X, Liu Y. Natural products modulate cell apoptosis: a promising way for the treatment of ulcerative colitis. *Front Pharmacol*. 2022;13:806148. doi:10.3389/fphar.2022.806148
58. Chen QL, Yin HR, He QY, Wang Y. Targeting the NLRP3 inflammasome as new therapeutic avenue for inflammatory bowel disease. *Biomed Pharmacother*. 2021;138:111442. doi:10.1016/j.biopha.2021.111442
59. Liu L, Dong Y, Ye M, et al. The pathogenic role of NLRP3 inflammasome activation in inflammatory bowel diseases of both mice and humans. *J Crohn's Colitis*. 2016:jjw219. doi:10.1093/ecco-jcc/jjw219